Plasma Dynamics Laboratory
Technical Report 71-3

November 1971

INSTABILITIES and TURBULENCE in HIGHLY IONIZED PLASMAS in a MAGNETIC FIELD

by J. H. NOON and W. C. JENNINGS

Semi Annual Status Report
NASA Grant No. 33-018-137
September 1, 1970 - February 29, 1972

Electrophysics Division
Rensselaer Polytechnic Institute
Troy, New York

SUMMARY

Experimental and theoretical work has been extended on the physical mechanisms of plasma turbulence and coherent instabilities. We believe turbulence may best be described in terms of parametric affects and experimental and theoretical results show that energy may be transferred in both directions of the frequency spectrum. Energy transfer to higher frequencies results in turbulence acting as a "safety-valve" against the growth of coherent, low frequency instabilities. Under conditions which are described in this report, energy may be transferred to lower frequencies, resulting in anomalously high diffusion rates. A linear theory has been applied to the drift instability in the Rensselaer HCD and reasonable agreement between predictions and experimental results has been obtained. In analyzing the predictions of this theory, close attention has been paid to the transition between the central core of the arc plasma, which is dominated by charged particle collisions, and the surrounding plasma medium which becomes neutral collision-dominated at different radii depending upon external parameters.

INTRODUCTION

This report is concerned with further experimental and theoretical work on instabilities and turbulence in the Rensselaer HCD device. Some of the results will be presented in three papers at the November meeting of the American Physical Society. These papers are: "Energy Transfer and Periodic Exchange by means of Three-Wave Interactions in a Highly Ionized Magnetoplasma", by G. S. Huchital, J. H. Noon, and W. C. Jennings; "Phase Properties of a Drift Wave in a Hollow Cathode Arc", by G. X. Kambic, J. H. Noon, and W. C. Jennings; "Feedback Stabilization of the Drift Instability in a Hollow Cathode Arc", by J. Stufflebeam, R. E. Reinovsky, J. H. Noon, and W. C. Jennings.

The major thrust of the recent work has been to obtain better physical understanding of the complex mechanisms leading to plasma turbulence and the growth of coherent instabilities. Particular attention has been placed on the transition in the Rensselaer device from the highly ionized central core, where charged particle collisions are dominate, to the outer region of plasma where neutral collisions control momentum transfer.

New diagnostic techniques have been developed to study the affects of three-wave interactions, which we view as the fundamental mechanism of plasma turbulence, and for monitoring the phase difference between density and potential fluctuations in the presence of a coherent instability. In addition, techniques have been refined to study the diffusion wave technique of monitoring cross-field diffusion which was described in our last report.

I. Diffusion Wave Techniques

A major problem in the field of plasma turbulence is the determination of the form of the energy spectrum. Several theories have been proposed[1-5], all of which predict a power-law spectrum in terms of the wavenumber k of the turbulent oscillations. Since it is much more expediant to measure an energy spectrum versus frequency rather than wavenumber, a dispersion relation derived for turbulent oscillations would be extremely helpful in applying any of the above theories to an experimental situation.

The diffusion wave theory, first derived by Golubev[6] and later applied to the HCD by Flannery and Brown[7] appears to meet this requirement at least for low frequency turbulent oscillations propagating in the radial direction. At this time an extension of the original diffusion wave theory is in progress and the results determined so far are included in this report. It is planned to include neutral-dominated and charged particle-dominated plasmas along with those plasmas whose radial diffusion can be described by anomalous or Bohm diffusion. Also diffusion wave theory will be extended to include higher frequency turbulent oscillations.

The previous report[8] (April 1971) examined, in detail, the diffusion wave theory as it applied to the hollow cathode discharge. Since that time several important aspects of a radially propagating diffusion wave have been experimentally examined. For completeness, the results of diffusion wave theory will be briefly presented.

If Bohm diffusion is assumed, the amplitude of a diffusion wave will appear as

$$N_B(r) = \frac{\text{const}}{T(r)} \exp - \int \frac{8\,B\omega}{QT(r)k_B}\,dr \qquad (1)$$

where

$T(r)$ = electron temperature (ev)

B = magnetic field strength

ω = frequency of diffusion wave

k_B = wave number of diffusion wave

Q = variable parameter

The wavenumber of the diffusion wave is theoretically predicted to follow the equation

$$k_B^4 + \left(\frac{32 \epsilon V_s B}{T(r) L Q} \right) k_B^2 + \left(\frac{8 B \omega}{Q T^2} \frac{\partial T}{\partial r} \right) k_B - \frac{64 B^2 \omega^2}{Q^2 T^2} = 0 \qquad (2)$$

where

ϵ = variable parameter

L = length of arc

V_s = $\left(\frac{e\ Te}{M^+}\right)^{1/2}$

For classical diffusion, the equations read as

$$N_e(r) = \frac{\text{const}}{T^{3/4}\, n_o(r)} \exp - \int \frac{\omega T^{1/2}}{2 C Q n_o k_c} dr \qquad (3)$$

and

$$k_c^4 \frac{Q C n_o}{T^{1/2}} + k_c^2 \left(\frac{2eV_s}{L} - \frac{5}{4} \frac{C n_o Q}{T^{3/2}} \frac{\partial^2 T}{\partial r^2} + \frac{45}{16} \frac{C n_o Q}{T^{5/2}} \left(\frac{\partial T}{\partial r}\right)^2 \right) + k_c \left(\frac{\omega}{4T} \frac{\partial T}{\partial r} - \frac{\omega}{2 n_o} \frac{\partial n_o}{\partial r} \right) - \frac{\omega^2 T^{1/2}}{4 C n_o Q} = 0 \quad (4)$$

where

C = constant

n_o = d.c. charged particle density

Experimentally, the amplitude of the diffusion wave is measured using a biased Langmuir probe whose signal is fed into an HP Wave Analyzer. The wave number of the diffusion wave is found by assuming $kr = \phi$ and measuring a radial phase shift ϕ using a PAR HR-8 lock in amplifier.

Equations 1-4 were derived under the assumption that the radial propagation of a diffusion wave can be considered axially uniform. This assumption was checked experimentally by monitoring the phase of a diffusion wave at two axial positions separated by approximately 18 inches. The results clearly bear out the assumption as shown in Fig. 1. The diffusion wave is propagating in the radial direction independent of axial position for all three frequencies of the diffusion wave tested.

The diffusion wave theory was derived and experimentally checked for the case of ion propagation[7]. The same equations should be applicable to the case of electron flux outward if the well known and often used

Note: The above equations appear slightly different from those in the previous report. These equations may be considered more complete.

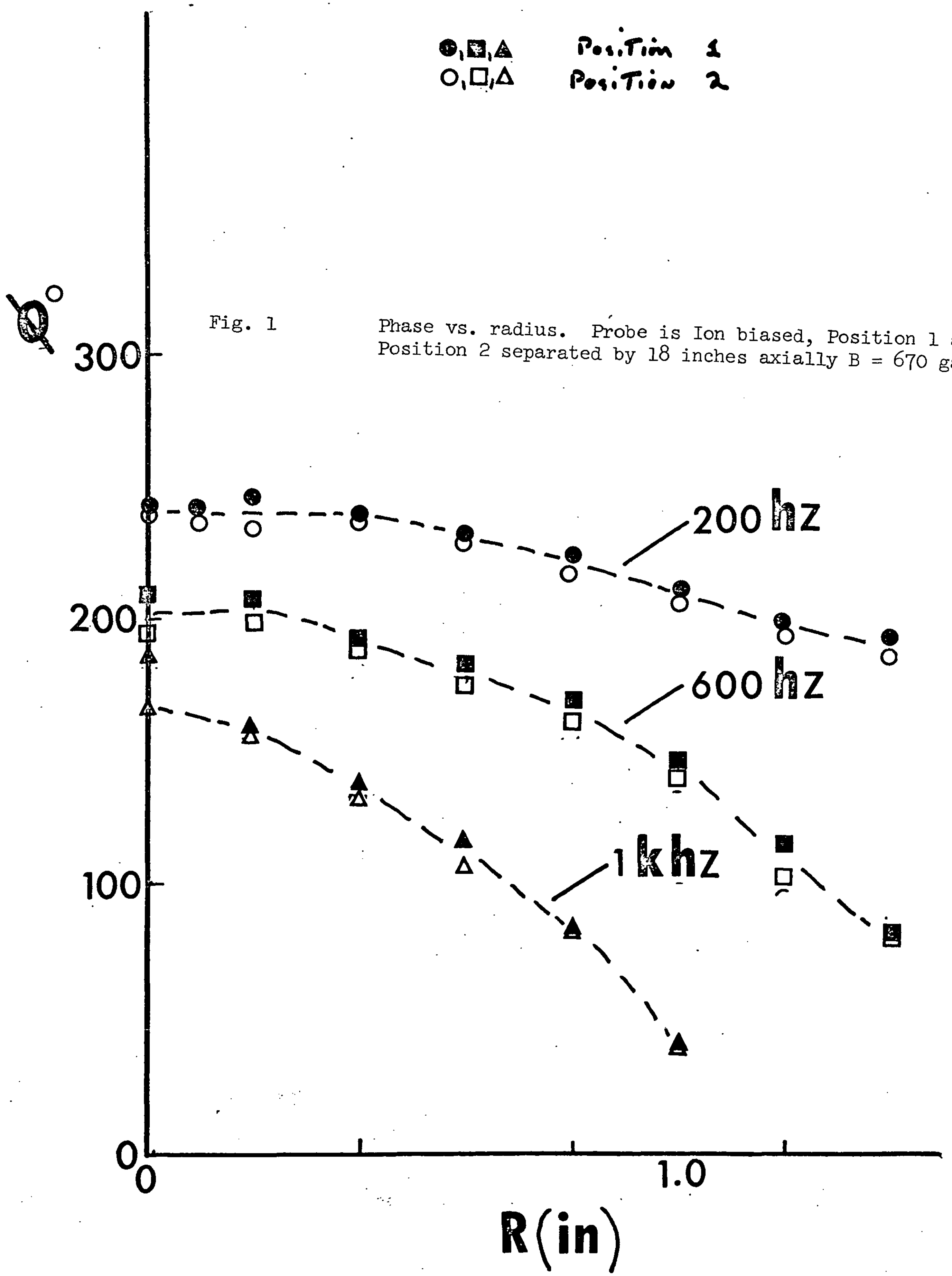

Fig. 1 Phase vs. radius. Probe is Ion biased, Position 1 and Position 2 separated by 18 inches axially B = 670 gauss.

assumption of ambipolar diffusion is true. Therefore in order to check the validity of the ambipolar diffusion assumption both ions and electron diffusion waves were monitored. Fig. 2 is a plot of the phase of electrons minus the phase of the ions associated with a diffusion wave versus radius. It can be seen that for low frequencies the phase difference between the ions and electrons remains constant at approximately 180°. This constant phase difference implies that both the ions and electrons are following the diffusion at the same rate. As the frequency of the diffusion wave is increased, the ions begin to lag the electrons by as much as 30°. It would appear therefore that the inertia of the ions begins to have an effect on ion propagation even at frequencies as low as 1000 Hz. For completeness Figure 3 contains the phase of the floating potential of the diffusion wave versus radial distance which appears close to being a constant.

At a magnetic field of approximately 670 gauss it was determined that the diffusion can be considered classical with a diffusion coefficient approximately ten times that predicted. Anomalous or Bohm diffusion was ruled out because different frequency diffusion waves needed vastly different variable parameters in order to fit theory to experiment. The experimental and theoretical cases can be seen in Fig. 4.

In order to extend the results of Flannery and Brown, the range of plasma conditions for which a diffusion wave was followed was increased. As a first step the magnetic field was varied over the range 600-1400 gauss. A direct comparison between theory and experiment became difficult at this point due to the possible effect of neutrals on the diffu-

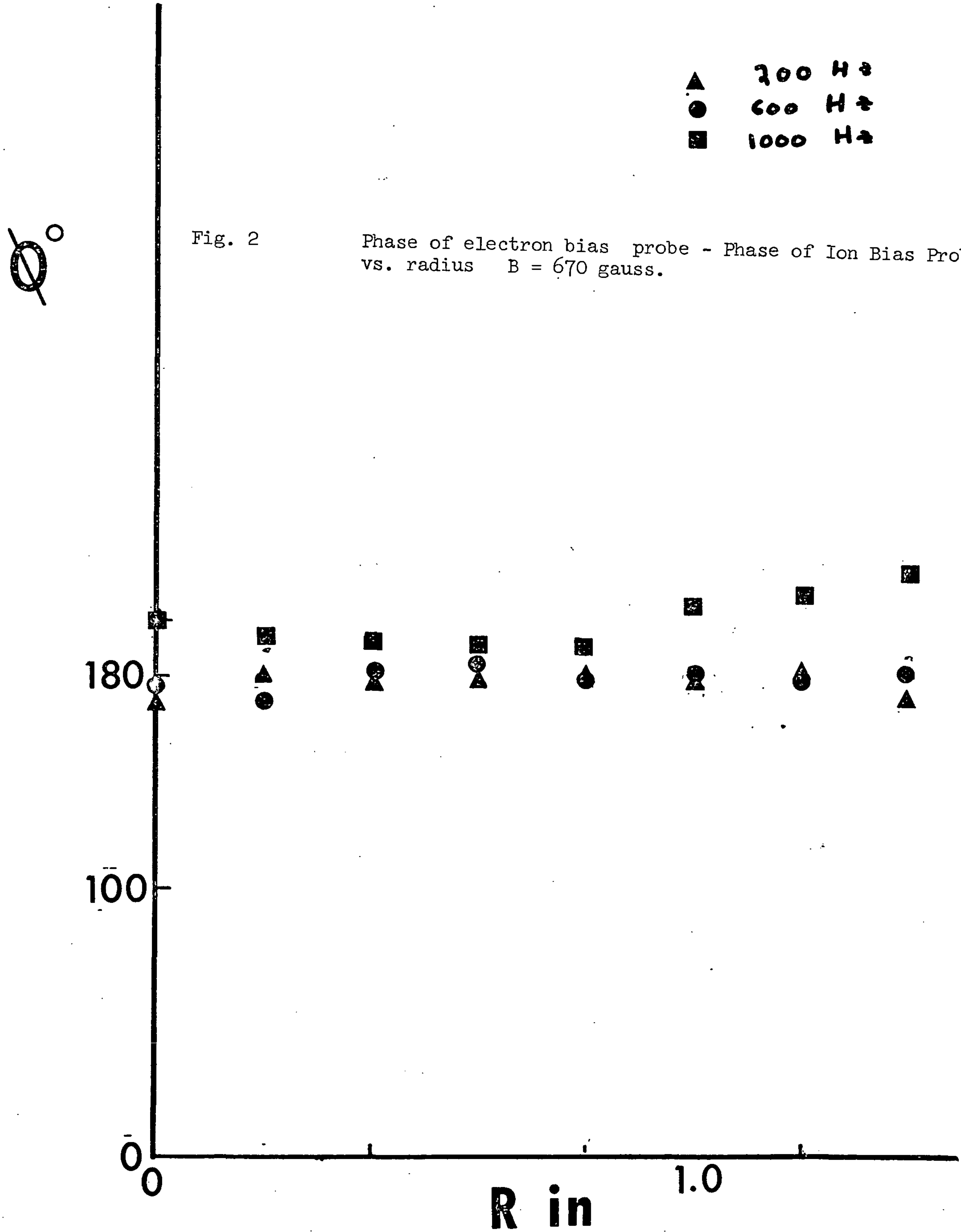

Fig. 2 Phase of electron bias probe - Phase of Ion Bias Probe vs. radius B = 670 gauss.

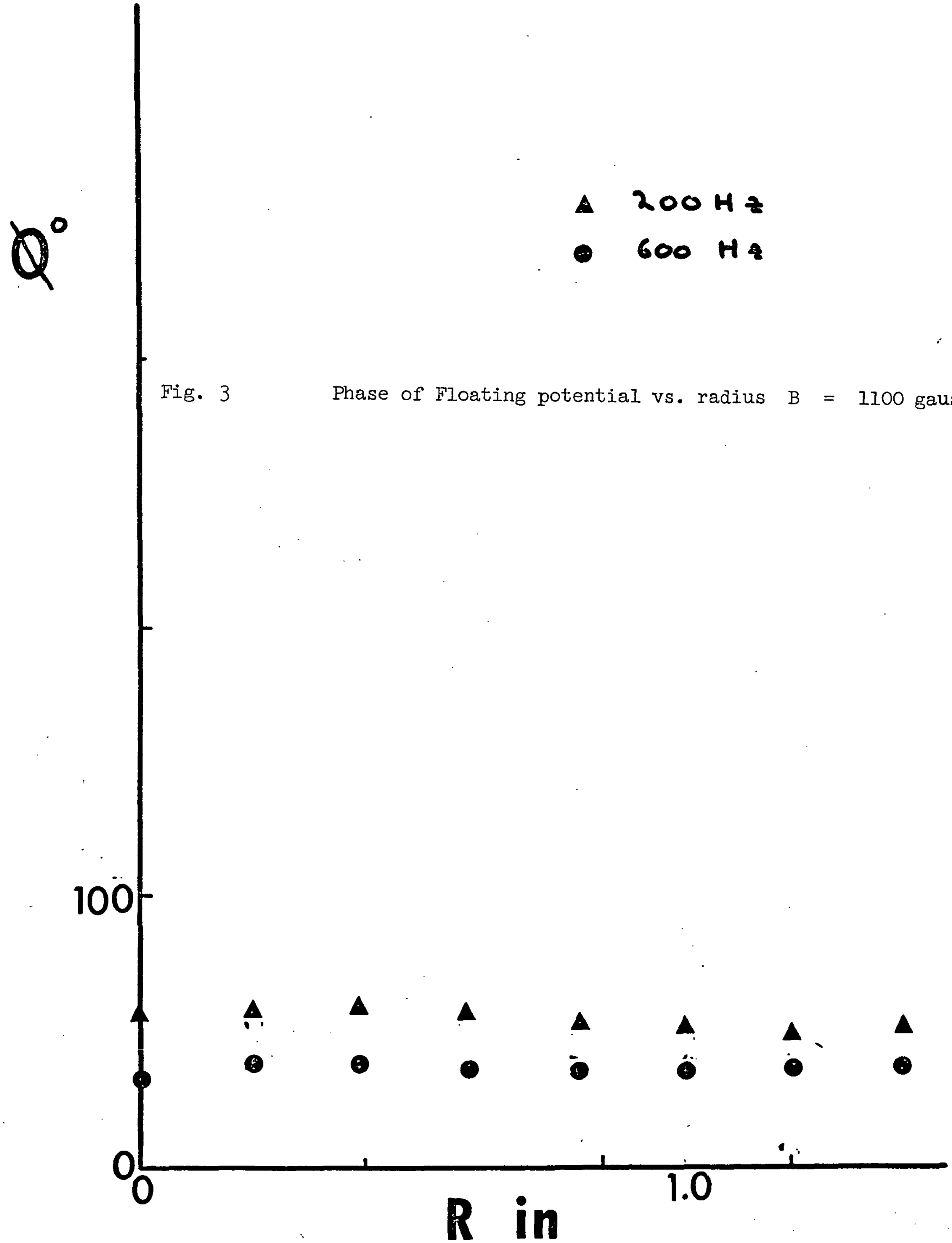

Fig. 3 Phase of Floating potential vs. radius B = 1100 gauss.

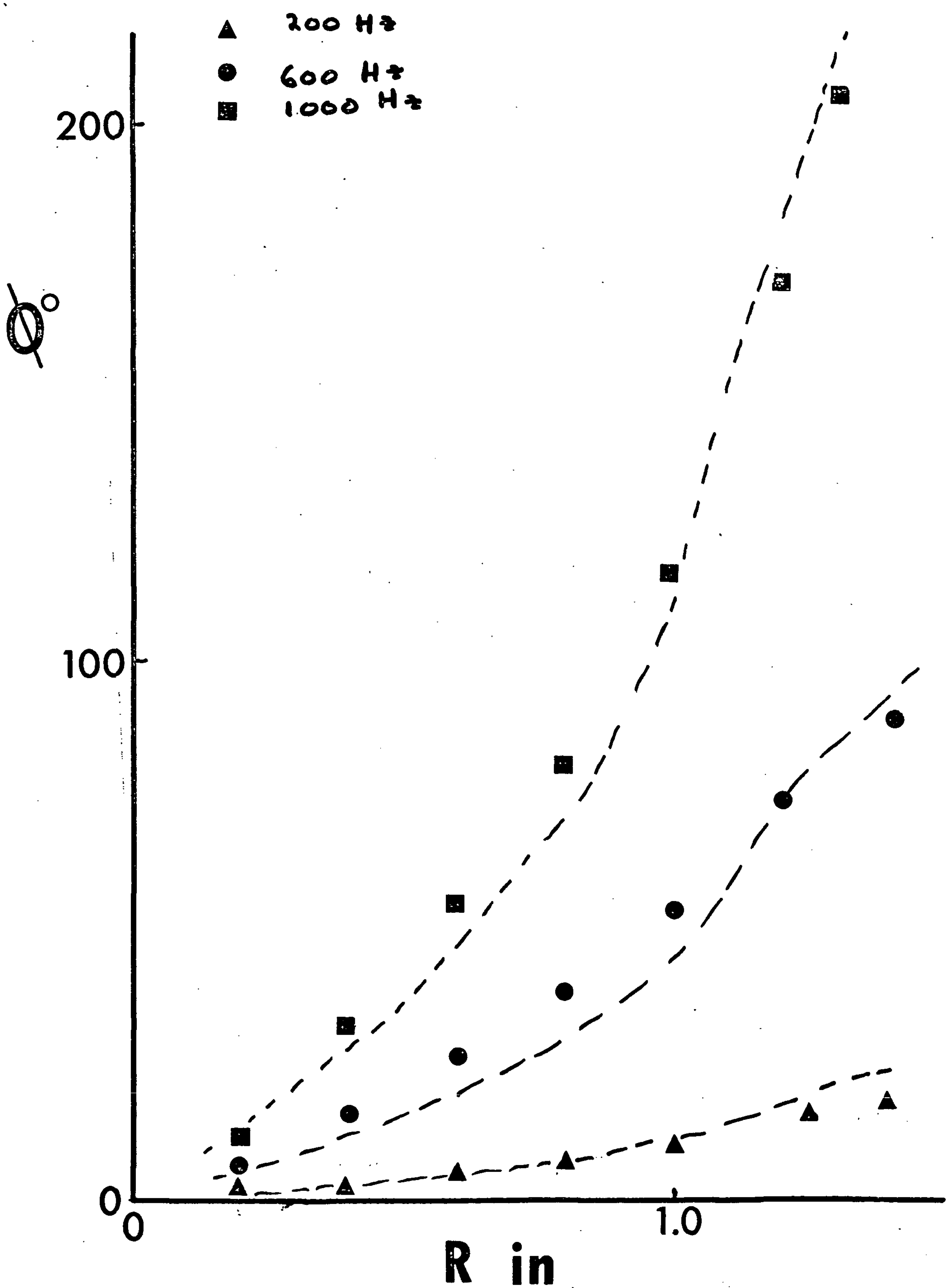

Fig. 4 Phase of ion oscillations vs. radius. Dashed lines - Theory, dots - experimental points $D \approx 10\, D_{CL}$, B = 670 gauss

sion process. Theoretically it was determined that if the percentage ionization were to drop below approximately 50%, the non-linearity in density of the diffusion wave under conditions of classical diffusion would disappear experimentally. Thus to the experimental observer, the propagation would appear very much like conditions of anamolous or Bohm diffusion. This would be due to the fact that once the plasma can no longer be considered highly ionized, neutral-charged particle collisions begin to dominate and the radial flux of charged particles changes from

$$\Gamma_{r1} = \left(K_1 \frac{\partial}{\partial r}(nT)\right) \nu_{EI} \qquad (5)$$

where V_{EI} = electron-ion collision frequency which is proportional to the charge particle number density to

$$\Gamma_{r2} = \left(K_2 \frac{\partial}{\partial r}(nT)\right) \nu_{EN} \qquad (6)$$

where V_{EN} = electron-neutral collision frequency which is not directly proportional to the number of charged particles.

Thus experimental results can become very confusing as one moves from regions in the plasma that are considered highly ionized outward into regions that may be weakly ionized. It is hoped that this difficulty can be overcome by including the transition from a charge-particle collision dominated plasma to a neutral dominated plasma in our theory. This work is being performed at this time.

In their hollow cathode arc, Flannery and Brown performed measurements in a comparatively quiescent plasma (Turbulence $\sim$ 2.5%). In our arc the level of turbulence varies radially and appears to have a large effect on the radial amplitude profile of a diffusion wave. Figure 5 plots the amplitude of a diffusion wave (ions are being followed) versus radius. The amplitude of the turbulence is monitored at the same time. It can be seen that radially there is a growth in the diffusion wave at the same radial position where the level of turbulence has increased. This effect is even more apparent when one monitors the electrons (Figure 6). This rise in the amplitude of the diffusion wave appears not to be explained by the existing theory. It is planned to include this effect, at least empirically, into the equations for the wavenumber of the diffusion wave. Increased accuracy in predicting the wavenumber of the diffusion wave is expected if the level of turbulence affects the radial propagation or diffusion of charged particles.

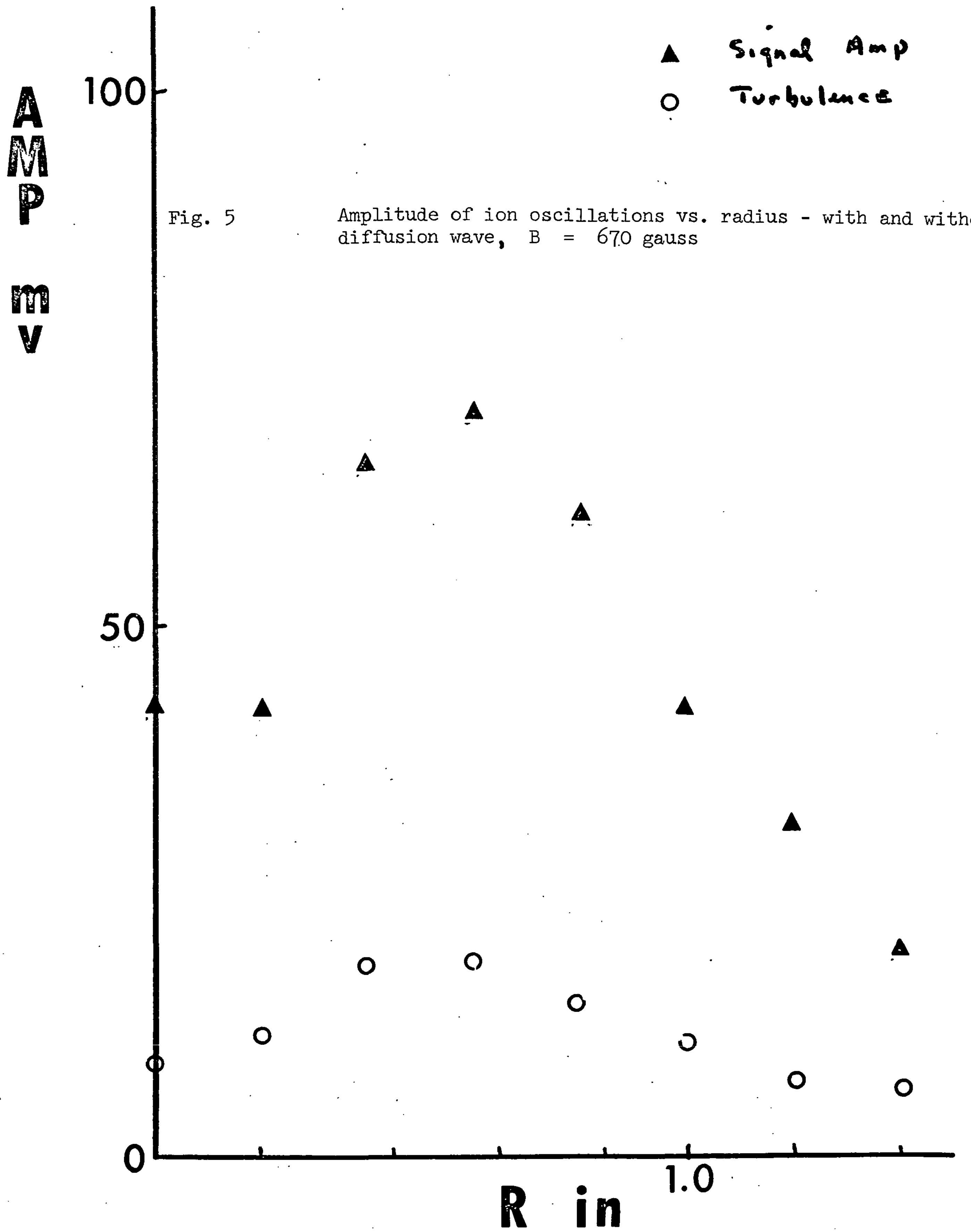

Fig. 5 Amplitude of ion oscillations vs. radius - with and without diffusion wave, B = 670 gauss

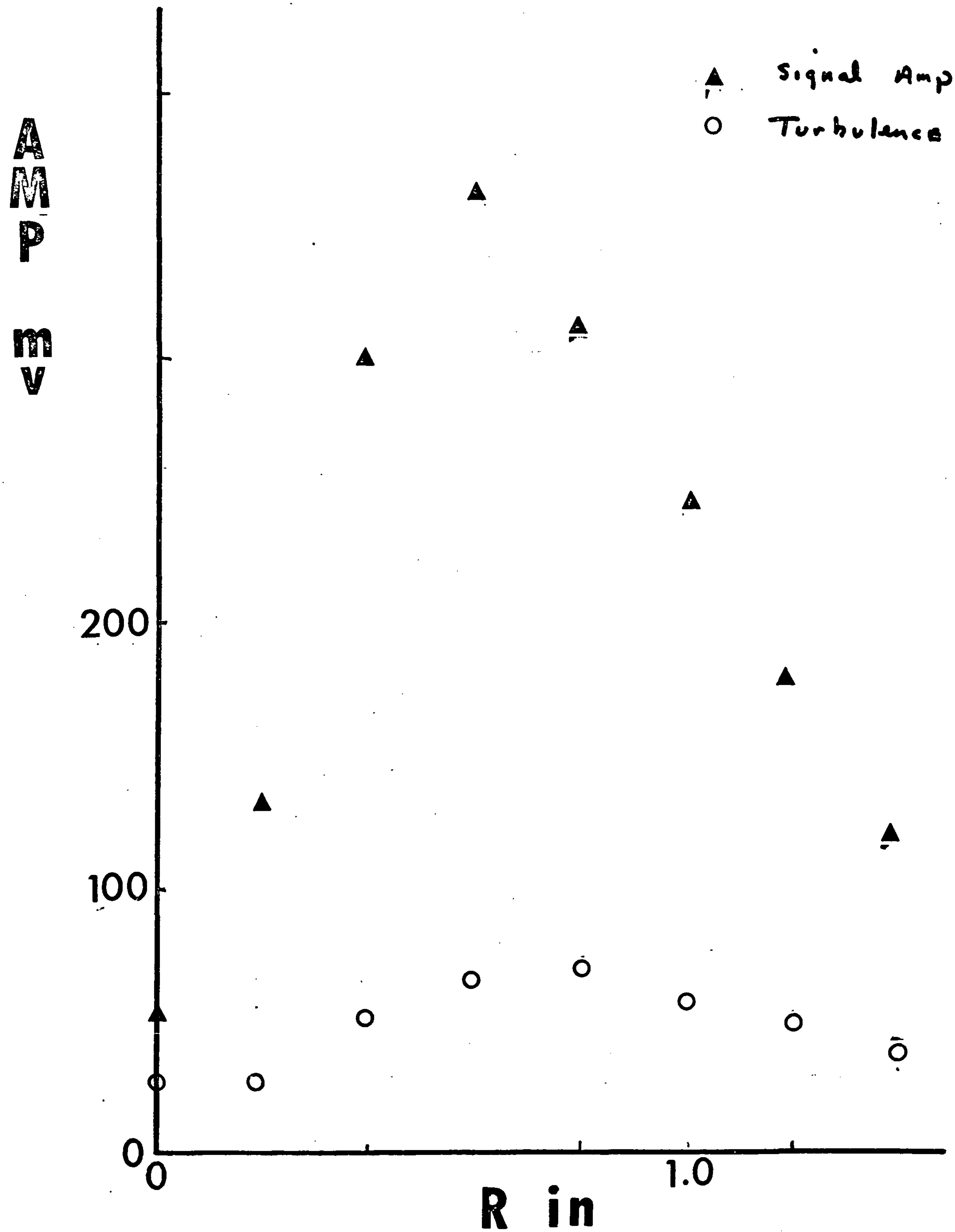

Fig. 6 Amplitude of electron oscillations vs. radius - with and without diffusion wave, B = 670 gauss.

II. Three Wave Interaction

At this time the proper direction of energy cascade in a turbulent spectrum is still a problem which has not been theoretically or experimentally decided.[4,9,10] In our last report it was shown that experimentally a non-linear three wave interaction can account for a transfer of energy either up or down the turbulent spectrum depending on plasma conditions. This phenomenon is analogous to parametric amplification affects observed in crystals.

In this report we attempt to place on more solid theoretical basis the possibility of wave-wave interactions leading to an energy transfer in either direction of the frequency spectrum. The goal of this work is to define the conditions necessary to determine the directions of the energy transfer. If transfer is towards higher frequencies, plasma turbulence, which we view as an infinite number of simultaneous parametric affects, may well act as a "safety valve" against the growth of strong coherent oscillations. However, if transfer occurs towards lower frequencies, the possibility exists for exceedingly high anomalous diffusion rates.

The previous report[8] considered a nonlinear wave-wave interaction derived from the continuity equation assuming classical diffusion.

It was found that by assuming a density $n = n_o + n_p$ where n_p is the density perturbation, $n_o \gg n_p$.

$$n_p = \sum_{j=1}^{3} n_j$$

$$n_j' = \tfrac{1}{2}\left(N_j(r,t)\,e^{i\psi_j} + N_j(r,t)\,e^{-i\psi_j}\right) \qquad \text{II-1}$$

where

$$\psi_j = k_j \cdot r - \omega_j t$$
$$k_3 = k_1 + k_2 \qquad \text{II-2}$$
$$\omega_3 = \omega_1 + \omega_2$$

coupling between the three oscillation n_1, n_2 and n_3 is predicted.

Three simultaneous coupled equations are formed for the amplitudes of the three perturbations

$$\frac{dN_1}{dt} = -\bar{X}_1 N_1 + \bar{Y}_1 N_2 N_3$$
$$\frac{dN_2}{dt} = -\bar{X}_2 N_2 + \bar{Y}_2 N_1 N_3 \qquad \text{II-3}$$
$$\frac{dN_3}{dt} = -\bar{X}_3 N_3 - \bar{Y}_3 N_1 N_2$$

where

$$\bar{X}_1 = \frac{2\epsilon V_s}{L} - 2An_0 - Bn_0\frac{\partial}{\partial r} - i\omega_1 - B\frac{\partial n_0}{\partial r} - D\left(2\frac{\partial n_0}{\partial r}\frac{\partial}{\partial r} + n_0\frac{\partial^2}{\partial r^2} - k_1^2 n_0 + \frac{\partial^2 n_0}{\partial r^2}\right)$$

$$X_2 = X_1 \text{ with 1 replaced by 2} \qquad \text{II-4}$$
$$X_3 = X_1 \text{ with 1 replaced by 3}$$

and

$$\bar{Y}_1 = -2A + B\frac{\partial}{\partial r} + D\left(\frac{\partial^2}{\partial r^2} - k_1^2\right)$$

$$\overline{Y}_2 = -2A + B\frac{\partial}{\partial r} - D\left(\frac{\partial^2}{\partial r^2} - k_2^2\right)$$

$$\overline{Y}_3 = 2A - B\frac{\partial}{\partial r} + D\left(\frac{\partial^2}{\partial r^2} - k_3^2\right)$$

where

$$A = C\left(\frac{1}{T^{3/2}}\frac{\partial^2 T}{\partial r^2} - \frac{3}{2\,T^{5/2}}\left(\frac{\partial T}{\partial r}\right)^2\right) \qquad \text{II-5}$$

$$B = \frac{3C}{2T^{3/2}}\frac{\partial T}{\partial r}$$

$$D = \frac{C}{T^{1/2}}$$

C = constant derived from the classical diffusion coefficient.

If we consider the wave-wave coupling as a second order effect and assume that the linear dispersion relation betwend ω and k is still satisfied, $X_1N_1 = X_2N_2 = X_3N_3 = 0$ since diffusion wave theory for one oscillation predicts a linear dispersion relation given by the equation $X_jN_j = 0$. Therefore neglecting the X_jN_j terms yields the three coupled equations

$$\frac{dN_1}{dt} = \overline{Y}_1 N_2 N_3$$

$$\frac{dN_2}{dt} = \overline{Y}_2 N_1 N_3 \qquad \text{II-6}$$

$$\frac{dN_3}{dt} = -\overline{Y}_3 N_1 N_2$$

The expression $\overline{Y}_j N_k N_l$ may be simplified by first assuming $\frac{\partial T}{\partial r} = 0$ and then using the expression that $X_j N_j = 0$. This leads to the fact that

$$-B k_j N_k N_l - 2D k_j \frac{\partial}{\partial r} (N_k N_l) = 0 \qquad \text{II-7}$$

where j, k, l are any perturbation of 1, 2, 3. With this knowledge it can be shown that $\overline{Y} N_k N_l$ can be written as $Y_j N_k N_l$ where

$$\begin{aligned} Y_1 &\approx -Dk_1^2 \\ Y_2 &\approx -Dk_2^2 \\ Y_3 &\approx +Dk_3^2 \end{aligned} \qquad \text{II-8}$$

If the third wave is initially absent (N_3 (r, 0) = 0) these equations can be be put in the form

$$\left(\frac{d \mu_3}{d \tau}\right)^2 = (1 - \mu_3^2) \quad (1 - p^2 \mu_3^2) \qquad \text{II-9}$$

where

$$\mu_3 = \left(\frac{Y_1}{Y_3}\right)^{1/2} \frac{N_3}{N_{10}} \quad ; \quad p = \left(\frac{Y_2}{Y_1}\right)^{1/2} \frac{N_{10}}{N_{20}}$$

$$\tau = (Y_3 Y_1)^{1/2} N_{10} t$$

$$N_1 (r,0) = N_{10}$$

$$N_2 (r,0) = N_{20}$$

This differential equation has the well known solution

$$\mu_3^2 = sn^2 (\tau, p) \qquad \text{II-10}$$

That is, there will be a periodic interchange of energy between the three perturbations. The periodicity is described by Jacobic Elliptic functions whose period is given by 4 K(p) where

$$K(p) = \int_0^{\pi/2} \frac{d\phi}{(1 - p^2 \sin^2\phi)^{1/2}} \qquad \text{II-11}$$

If the quantity p = 1 the differential equation II-7 reduces to

$$\left(\frac{d\mu_3}{d\tau}\right) = 1 - \mu_3^2 \qquad \text{II-12}$$

The solution of which is

$$\mu_3 = \text{Tanh}\,(\tau) \qquad \text{II-13}$$

That is, there will be a transfer of energy from perturbations 1 and 2 into 3, causing the third wave to grow at the expense of the other two.

These results agree with those derived by Das[11] who used a different approach and assumed a homogeneous plasma.

It is possible that the transfer of energy in a three wave interaction may be used to describe the direction of cascade of energy (up or down in frequency) in a turbulent plasma.

If we assume that either ω_1 or ω_2 is initially absent ($N_1(r,0) = 0$ or $N_2(r,0) = 0$) we find for $N_2(r,t)$ ($N_2(r,0) = 0$)

$$\left(\frac{d\mu_2}{d\tau}\right)^2 = (1-\mu_2^2)(1-p_2^2\mu_2^2)$$

$$\mu_2 = \left(\frac{\gamma_3}{\gamma_2}\right)^{1/2} \frac{N_2}{N_{30}} \; ; \qquad p_2 = \left(\frac{\gamma_1}{\gamma_3}\right)^{1/2} \frac{N_{30}}{N_{10}} \qquad \text{II-14}$$

$$\tau = (\gamma_2\gamma_3)^{1/2} N_{10}\, t$$

and for N_1 (r,T) (N_1 $(r,0) = 0$)

$$\left(\frac{d\mu_1}{d\tau}\right)^2 = (1-\mu_1^2)\,(1-p_1^2\mu_1^2)$$

$$\mu_1 = \left(\frac{Y_3}{Y_1}\right)^{1/2} \frac{N_1}{N_{30}} \; ; \qquad p_1 = \left(\frac{Y_2}{Y_3}\right)^{1/2} \frac{N_{30}}{N_{20}} \qquad \text{II - 15}$$

$$\tau = (Y_3 Y_1)^{1/2} N_{20}\, t$$

For all three cases ($N_1(r,0) = 0$, N_2 $(r,0) = 0$ or N_3 $(r,0) = 0$) a transfer of energy will occur when $p = 1$. At that time the wave that was initially absent will grow, taking its energy from the original two waves that interacted to form the third.

When $p_1 = 1$

$$\left(\frac{N_{30}}{N_{20}}\right)^2 = \frac{Y_3}{Y_2} \approx \frac{k_3^2}{k_2^2} > 1$$

$p_2 = 1$

$$\left(\frac{N_{30}}{N_{10}}\right)^2 = \frac{Y_3}{Y_1} \approx \frac{k_3^2}{k_1^2} > 1 \qquad \text{II - 16}$$

$p_3 = 1$

$$\left(\frac{N_{10}}{N_{20}}\right)^2 = \frac{Y_1}{Y_2} \approx \frac{k_1^2}{k_2^2} < 1$$

Assuming a positive group velocity, if $\omega_3 > \omega_2 > \omega_1$ then $k_3 > k_2 > k_1$.

Therefore if the wave at ω_1 is initially absent, (case $p_1 = 1$), in order for energy to be transferred down in frequency $N_{30} > N_{20}$ or the amplitude spectrum of oscillations must rise at some point with increased frequency.

The same is true for a transfer of energy into a "middle" frequency ω_2 (case $p_2 = 1$) or upwards in frequency into the wave at ω_3 (case $p_3 = 1$).

To summarize, the possibility for energy exchange depends on the resonance conditions $\omega_1 + \omega_2 = \omega_3$, $k_1 + k_2 = k_3$. If these conditions are met the possibility exist for a periodic interchange of energy between the three waves. If along with this interaction the frequency spectrum does not decrease monotonically, there exists the possibility of an energy transfer either up or down the frequency spectrum.

Table 1 summarizes the possibilities existing with different shape amplitude spectra. It should be remembered that these results were derived neglecting the effect of any temperature gradients which may shift the final results slightly.

TABLE 1

Possibility for Direct Transfer of Energy

Shape of Amp. Spectrum	Interacting Frequencies $\omega_1 + \omega_2$, ω_3 initially absent	$\omega_2 + \omega_3$, ω_1 initially absent	$\omega_1 + \omega_3$, ω_2 initially absent
$N_1 > N_2 > N_3$	X	X	X
$N_1 > N_3 > N_2$	X	ω_1	X
$N_2 > N_1 > N_3$	ω_3	X	X
$N_2 > N_3 > N_1$	ω_3	X	ω_2
$N_3 > N_1 > N_2$	X	ω_1	ω_2
$N_3 > N_2 > N_1$	ω_3	ω_1	ω_2

III. A Study of Phase Properties of a Drift Wave

A. Introduction

In this section the latest experimental and theoretical work performed on the drift instability in the Rensselaer arc is presented. A theoretical relationship has been developed for the phase difference between space potential and ion density oscillations associated with this instability. Experimental techniques havè been developed for studying this relationship, and experimental results for variation of the phase difference as a function of plasma parameters are presented.

B. Experiment

The Rensselaer arc produces a highly ionized magnetoplasma which is unstable in certain pressure and magnetic field regimes to a low frequency drift instability which is driven by density and temperature gradients (11). The drift wave has been identified as an $m = 1$ azimuthal mode propagating in the electron diamagnetic direction through the use of the rotatable azimuthal probe (12) (Figure 7).

The operating parameters at which the drift wave has been studied are: magnetic field 1500-2200 gauss; gas flow = .1 cc-atm/sec; neutral background pressure $p_1 = 1 \times 10^{-4}$ torr, axial current = 20 amps, central maximum particle densities $n_o = 10^{14}$ cm^{-3}, and maximum electron temperatures of 5-10 ev. Plasma diagnostics were done using tungsten Langmuir probes that were coaxially shielded. Configurations for both radial and azimuthul movements of the probe are available.

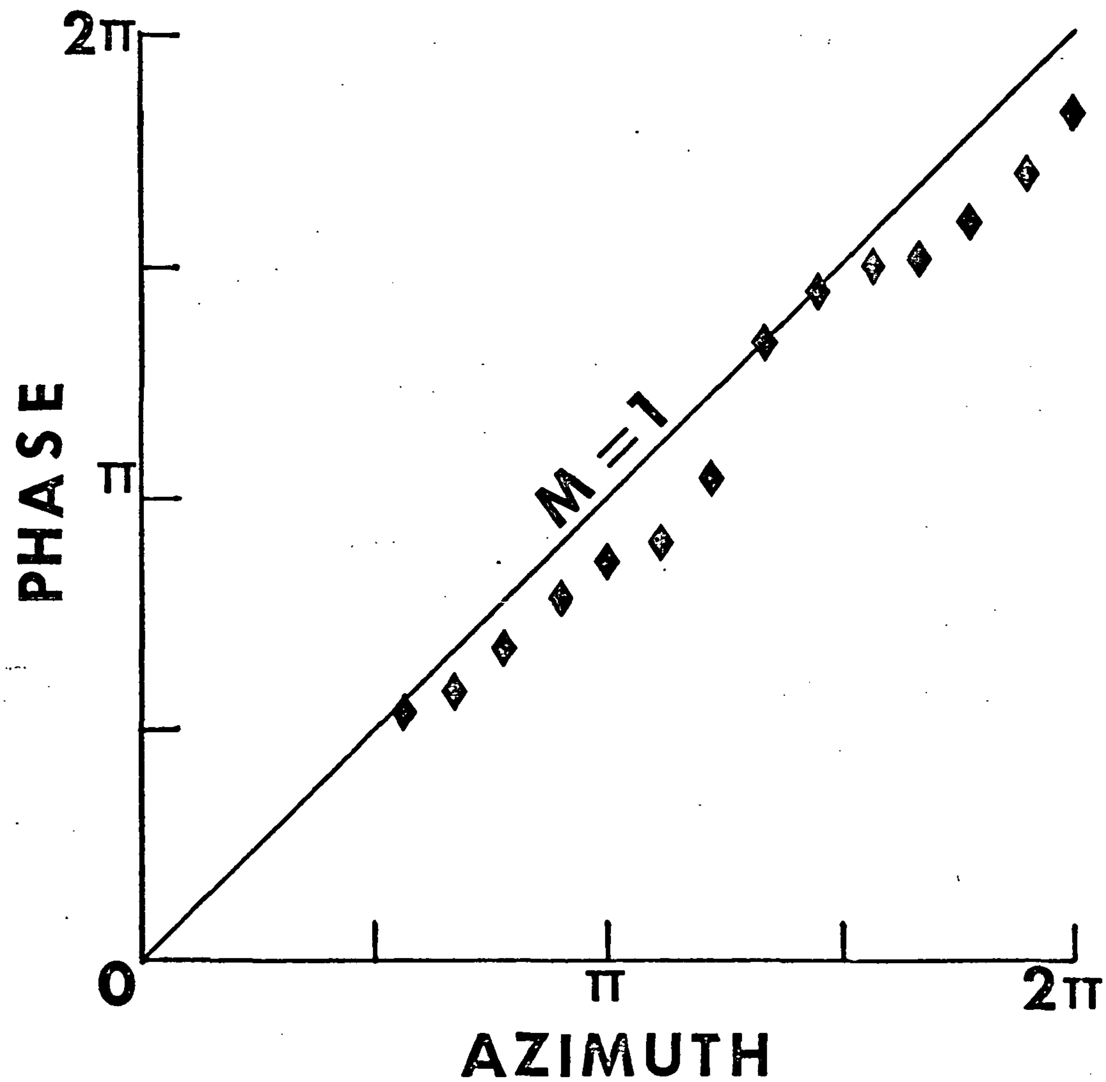

Figure 7

Phase Shift of drift wave as a function of azimuth. Direction of wave is electron diamagnetic.

Instrumentation for AC measurements includes a PAR Model 100 correlator, PAR Model 102 Fourier analyzer and PAR Model HR-8 lock-in amplifier, used as a phase sensitive detector.

The radial region in which the drift wave has been studied is 1.5 cm to 4.5 cm from the plasma center. Probe measurements were not made closer than 1 cm from arc center due to the high current density core. At $r = 1.5$ cm, the drift wave is at its maximum amplitude for the conditions examined. One probe is fixed at this radius to provide a reference signal for phase measurements. A second probe located at the same azimuthul position is moved radially and measurements are made of the floating potential, fluctuation amplitude, fluctuation frequency, turbulence level and phase difference between fluctuation signals on the two probes. An I-V characteristic curve is also taken at each point to provide DC plasma parameters. The probes are axially separated by 1 cm, but this has been shown to have no effect on the measurements reported.

A set of conditions at which the drift wave was a very sharp instability was chosen as a standard to reference further data as external parameters were varied. These conditions were $B = 1780$ gauss, current $I_{ARC} = 20$ amps, gas flow rate of .1 cc - atm/sec. and pressure $p_1 = 1 \times 10^{-4}$ Torr.

Figure 8 shows a typical plot of the phase difference as a function of radius between the two probes at floating potential. A positive phase angle implies that the reference probe signal lags the other signal. Fig. 9 shows the measured phase difference vs. radius when the moveable probe is biased into the ion saturation region. By substracting the phase in Fig. 8 from that in Fig. 9, the phase difference between the density and potential oscillations at each point in the plasma is obtained. This is

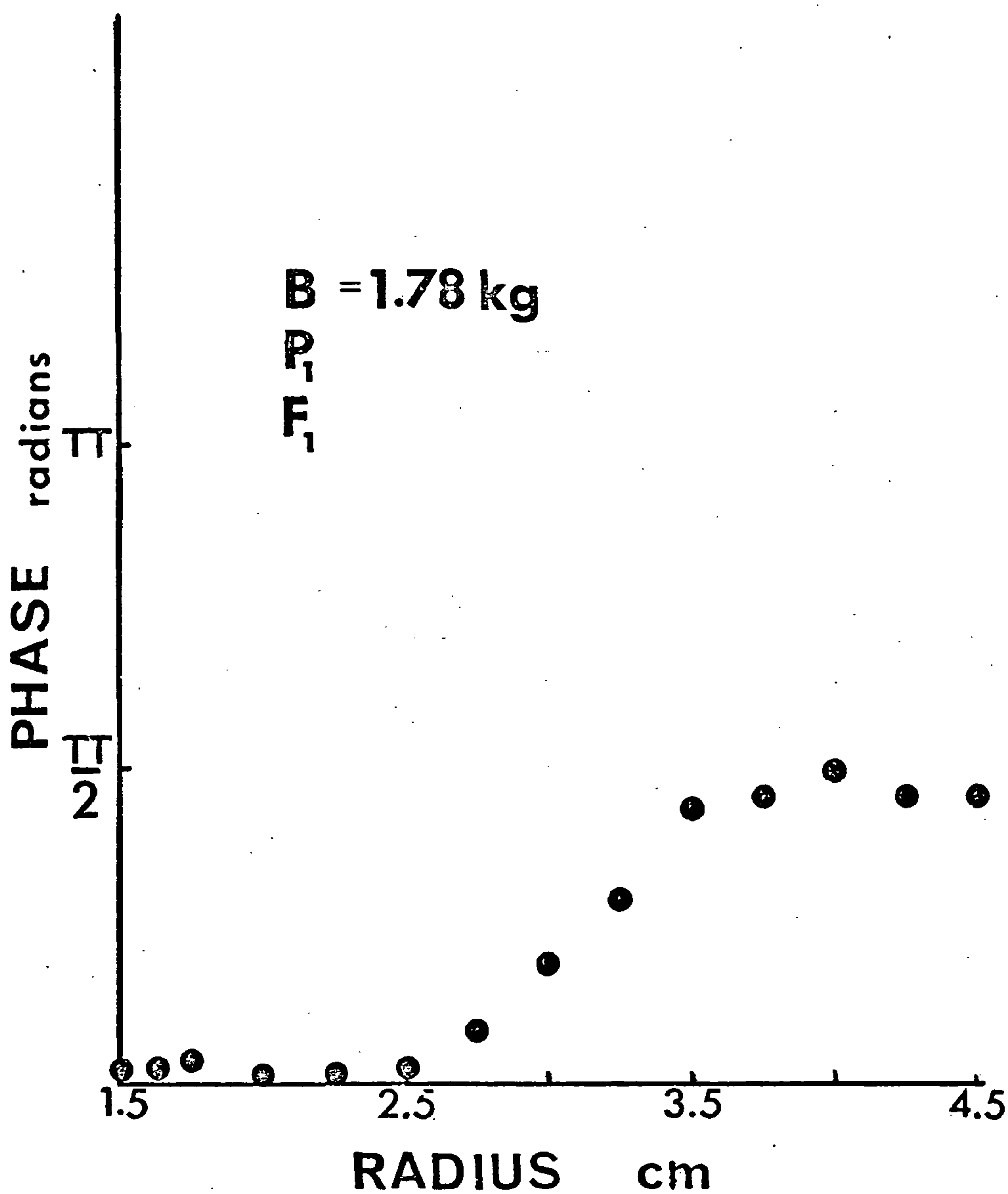

Figure 8

Phase of movable probe at floating potential as a function of radius. Standard drift wave conditions.

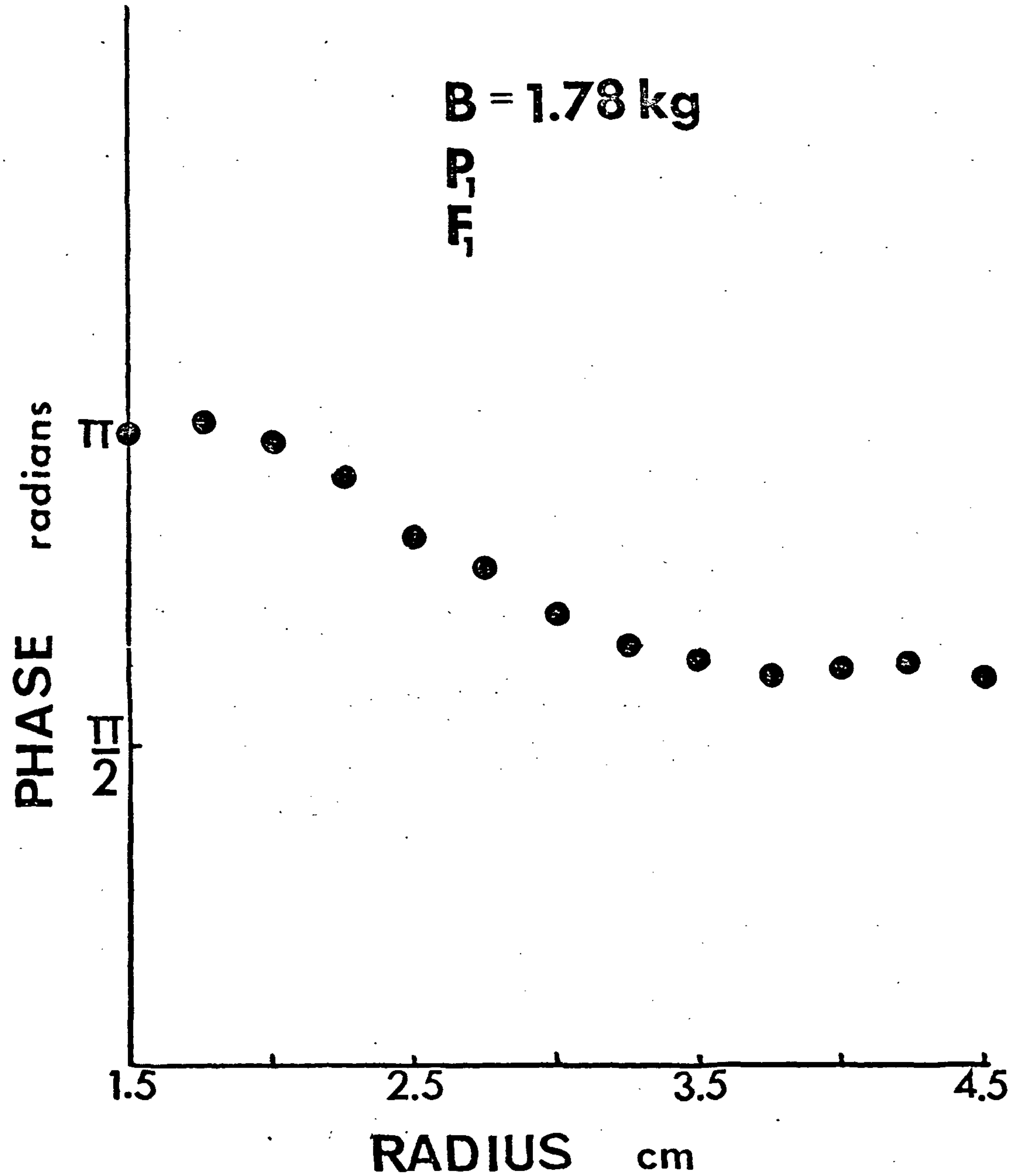

Figure 9

Phase of movable probe biased into the ion saturation region as a function of radius at standard drift wave conditions.

shown in Fig. 10. Experiments confirmed that the shape and magnitude of the measured phase shift is independent of the placement of the reference probe. Externally controlled arc parameters were then changed to observe variations in this phase difference as a function of these changes. The quantities varied were input gas flow rate, neutral background pressure, and magnetic field.

1) Variation of flow rate

The gas flow through the cathode was varied by a flow valve. The amplitude of the potential fluctuations decreased as the flow rate increased as indicated in Table I.

Table I

Flow $f_{cathode}$ (atm-cc/sec)	Potential Amplitude ϕ_i^* (at r = 1.5 cm)
.1	1
.1 + 15%	.87
.1 + 30%	.66

This decrease was consistent for all measured points. The ion density fluctuations did not show the same type of decrease in size as the potential fluctuations, as shown in Figure 11.

The phase differences between ion density and potential oscillations for these flow conditions is shown in Figure 12. No consistent change was observable.

Figures 13, 14 and 15 show respectively ion density, electron temperature and space potential gradients. Figure 13 shows the ion density gradient for the three flow conditions. Increased flow led to enhancement of the central density as well as a smoother density gradient. The

* Normalized to f_c = .1 atm - cc/sec

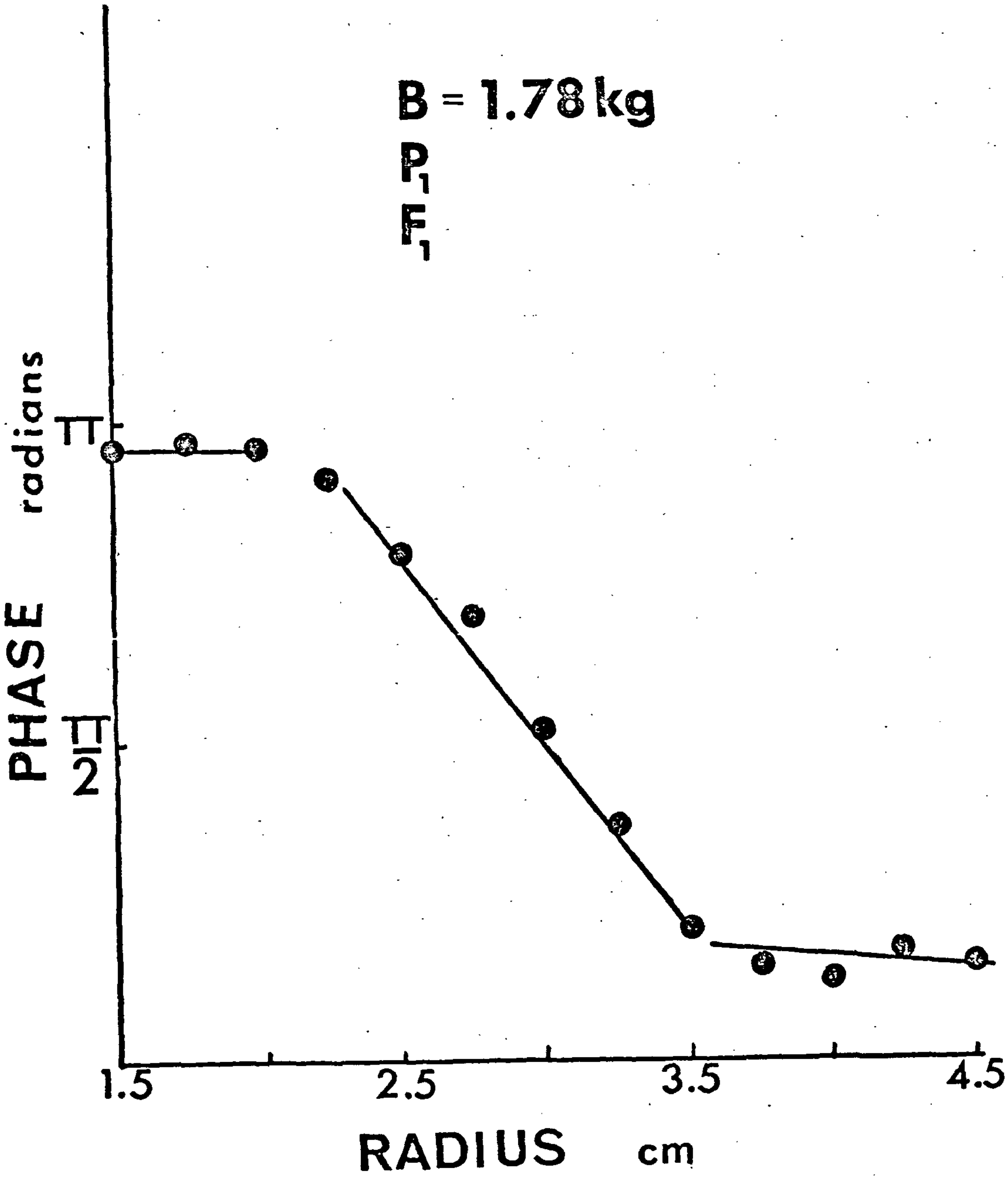

Figure 10

Fig. 9 minus Fig. 8. Phase difference between ion density and potential fluctuations as a function of radius. Standard drift wave conditions.

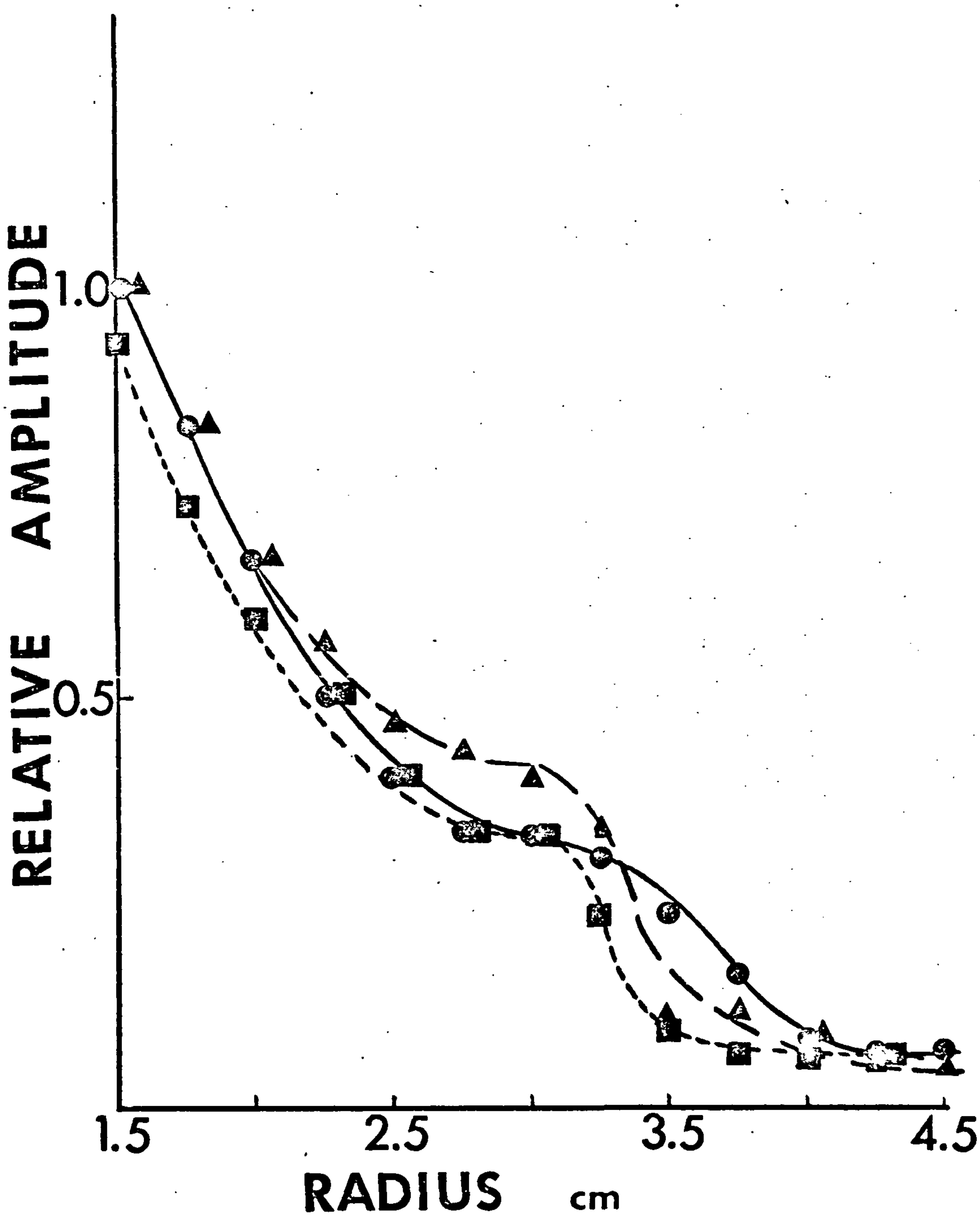

Figure 11

Amplitude of ion density fluctuations as a function of radius. Flow rate parameter.

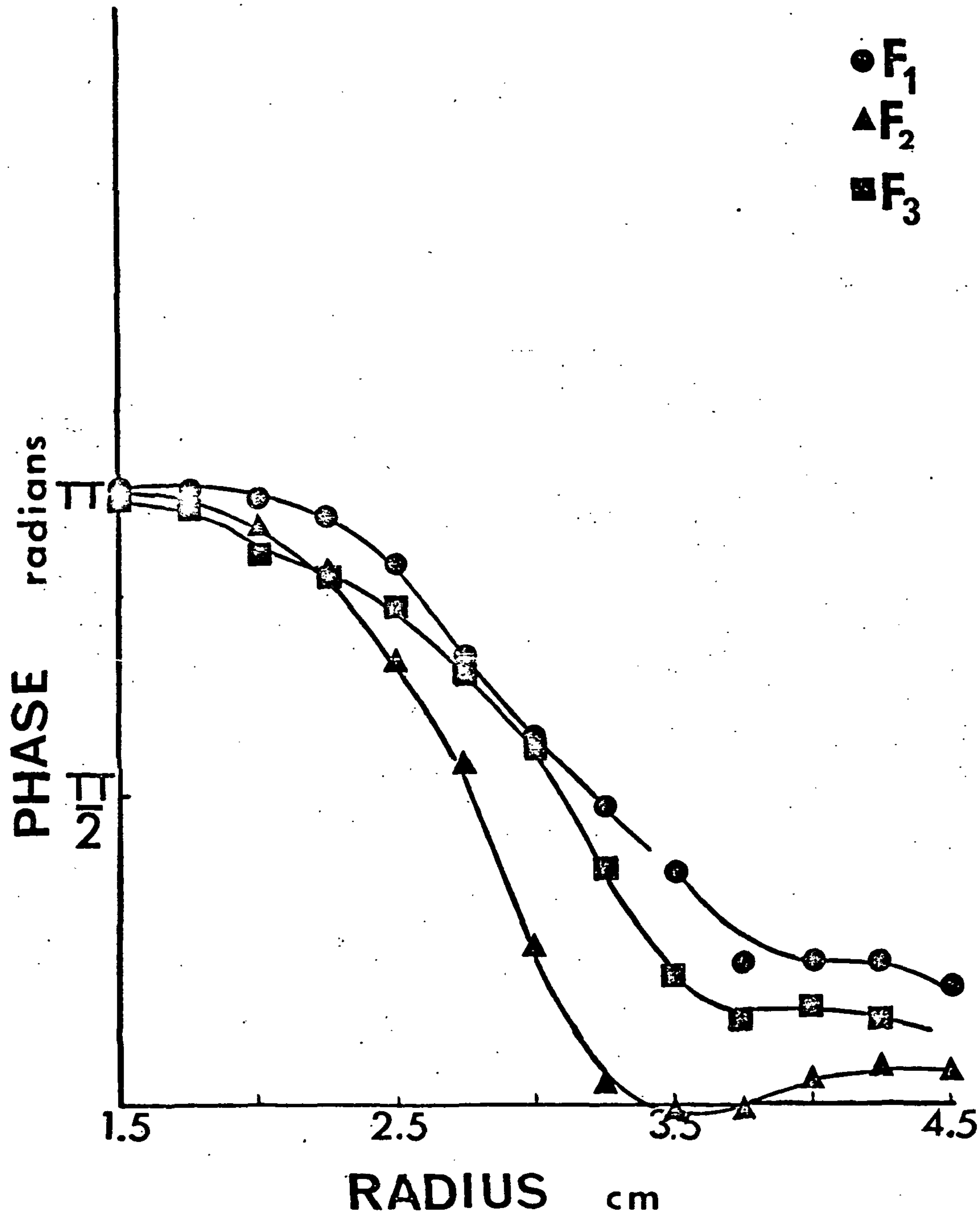

Figure 12

Phase difference between density and potential. Flow rate parameter.

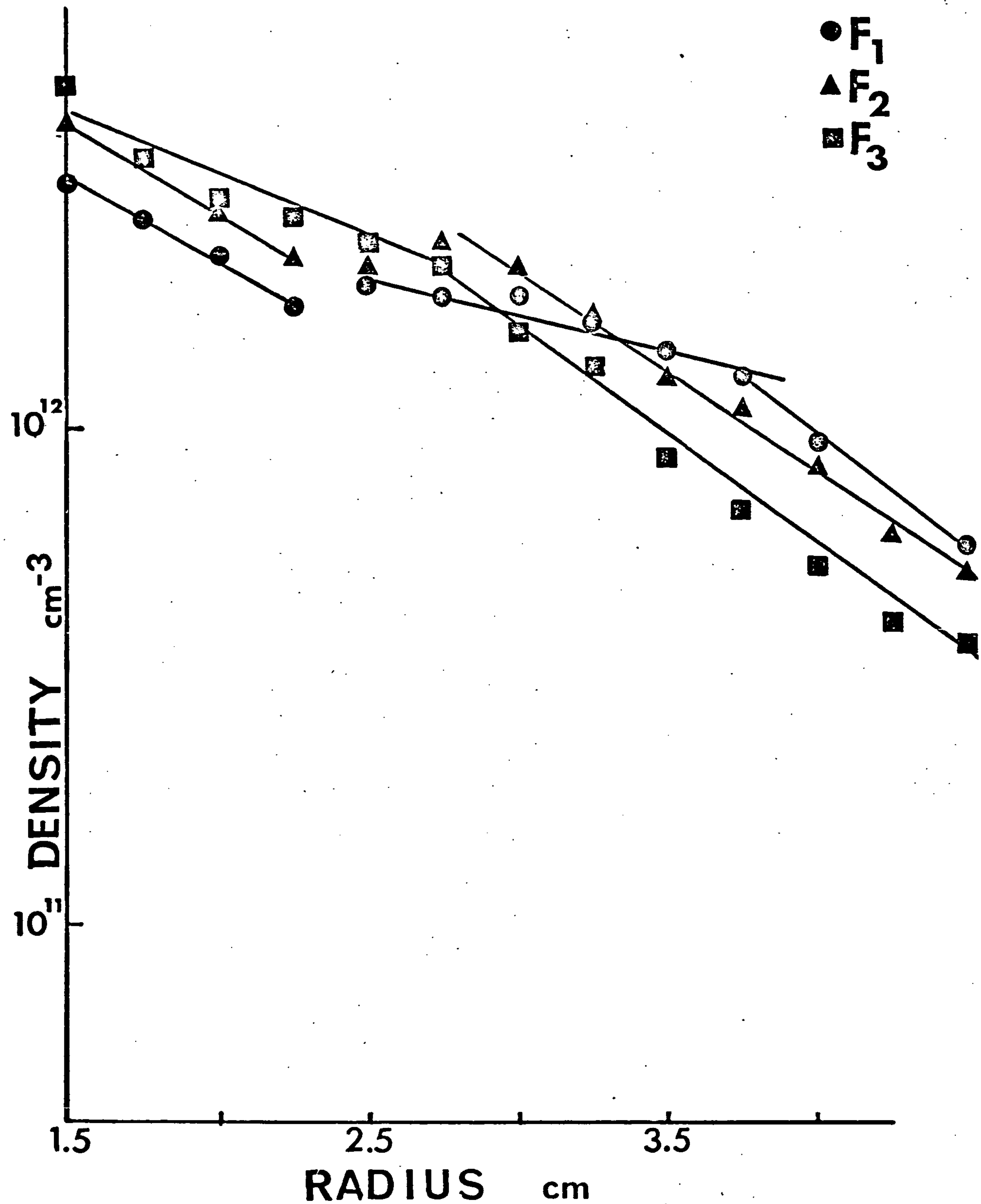

Figure 13

Ion density vs. radius. Flow rate parameter.

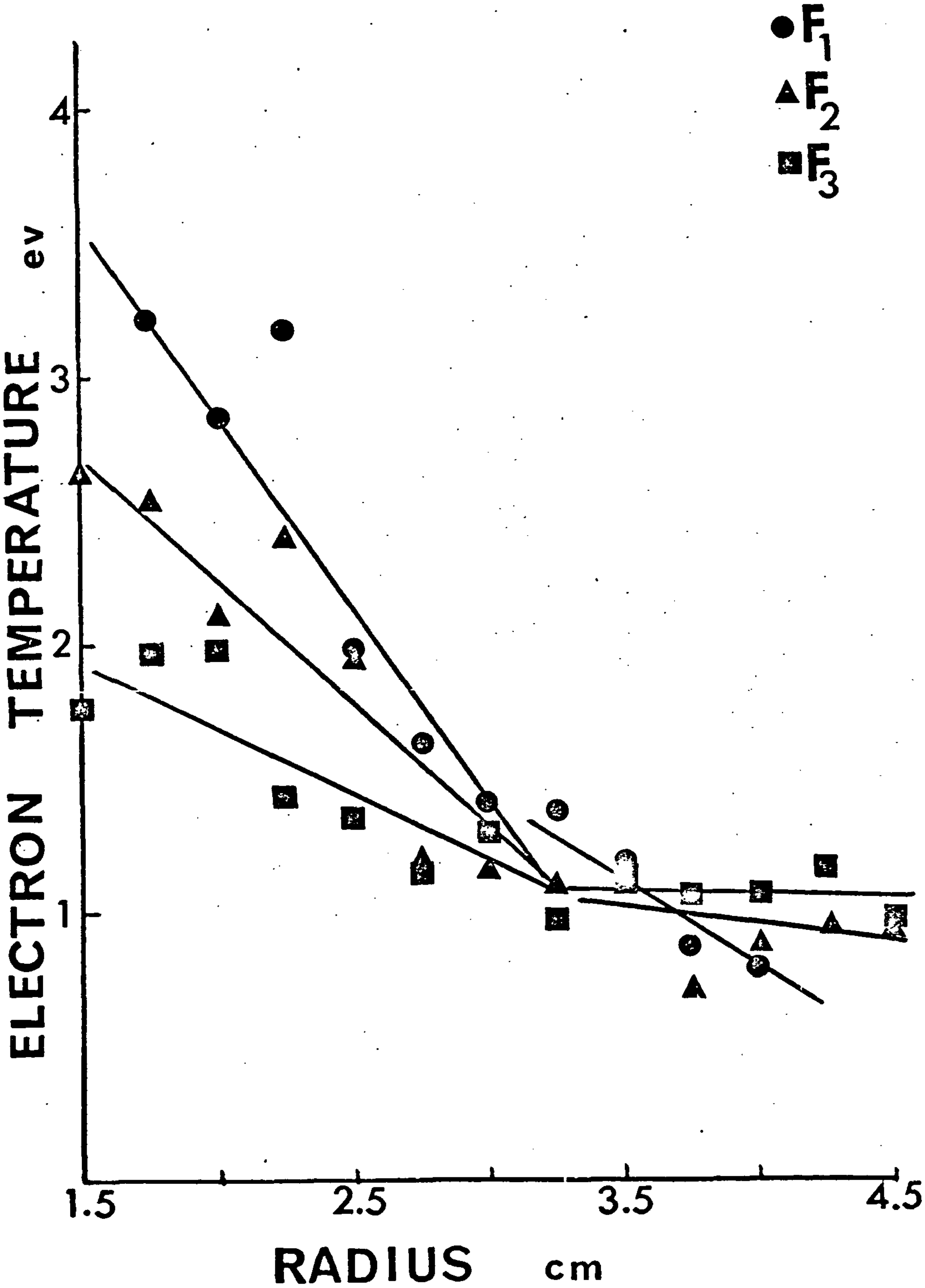

Figure 14

Electron temperature vs. radius. Flow rate parameter.

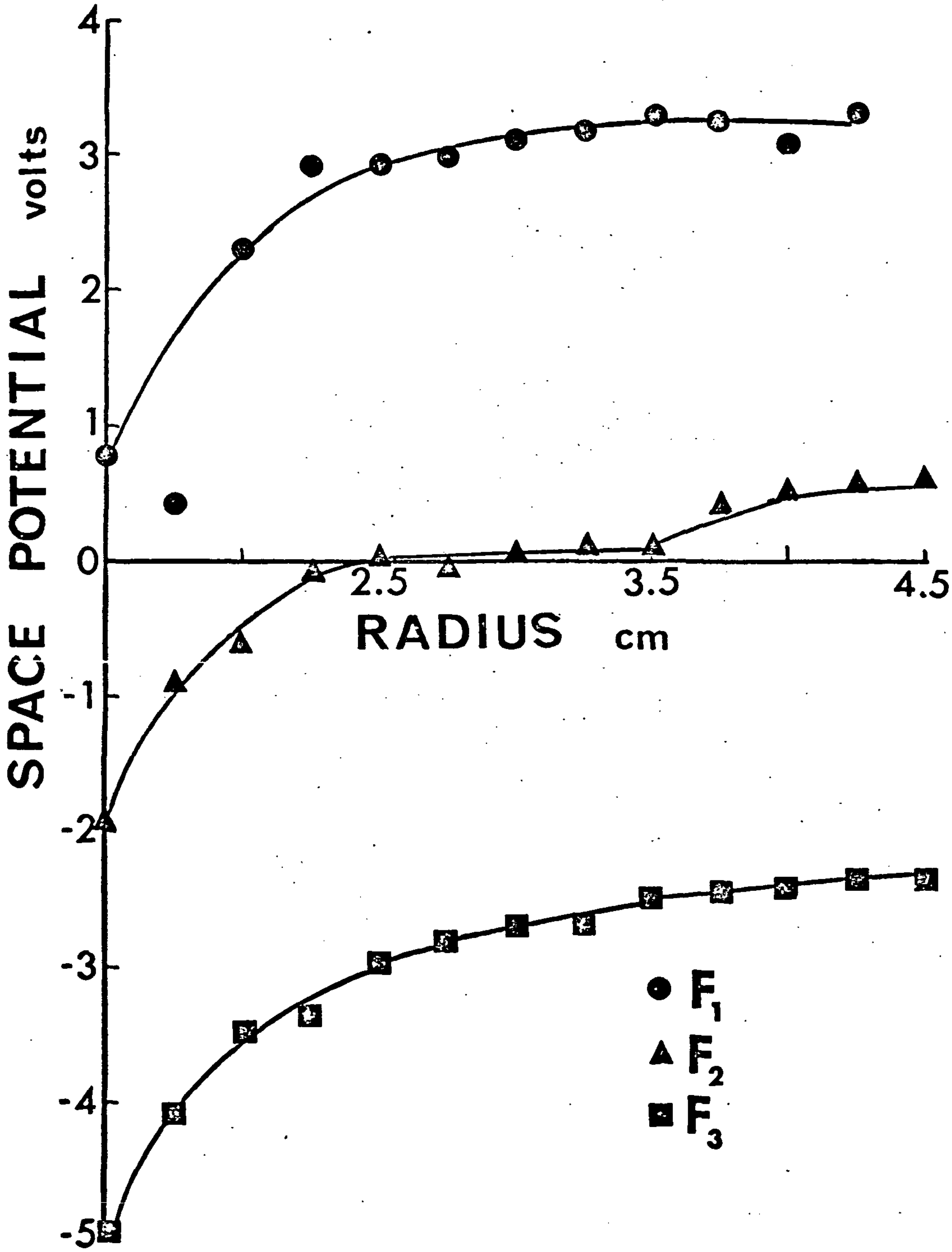

Figure 15

Space Potential vs. radius. Flow rate parameter.

increased flow also produced a higher neutral density near the walls of the plasma. Figure 14 shows the variation of the electron temperature with radius. The central temperature fell as the flow increased. There was a cooling effect due to electron-ion collisions close to the core.

In Figure 15, the variation of the space potential is shown. The potential gradient did not vary while the absolute value of the space potential shifted downwards. The variation of this absolute value will be seen to be non-significant in the Section (C) of this report.

2) Variation of Neutral Pressure

Large gate values were used to control the neutral background pressure while the gas flow into the system was kept constant. Three measured neutral pressures were examined $p_1 = 1 \times 10^{-4}$, torr $p_2 = 1.6 \times 10^{-4}$ torr, and $p_3 = 3 \times 10^{-4}$ torr. The phase differences between ion density and potential is shown in Figure 16 as a function of radius and pressure. This should be compared with Fig. 12. The phase difference at $r < 3$cm showed a consistent change with variation of pressure. The amplitude of both density and potential fluctuations decreased consistently in size as the pressure increased. This was true at all radii at which measurements were taken.

Figures 17, 18 and 19 show variations of respectively ion density, electron temperature and space potential. Note that the electron temperature and ion density (at $r > 3$cm) were depressed as the pressure increased. This was of course due to the large number of neutrals now present at the walls. The electron temperatures decreased because of the cooling effects of an increased ion-neutral collision frequency. The relative space potential gradient changed little.

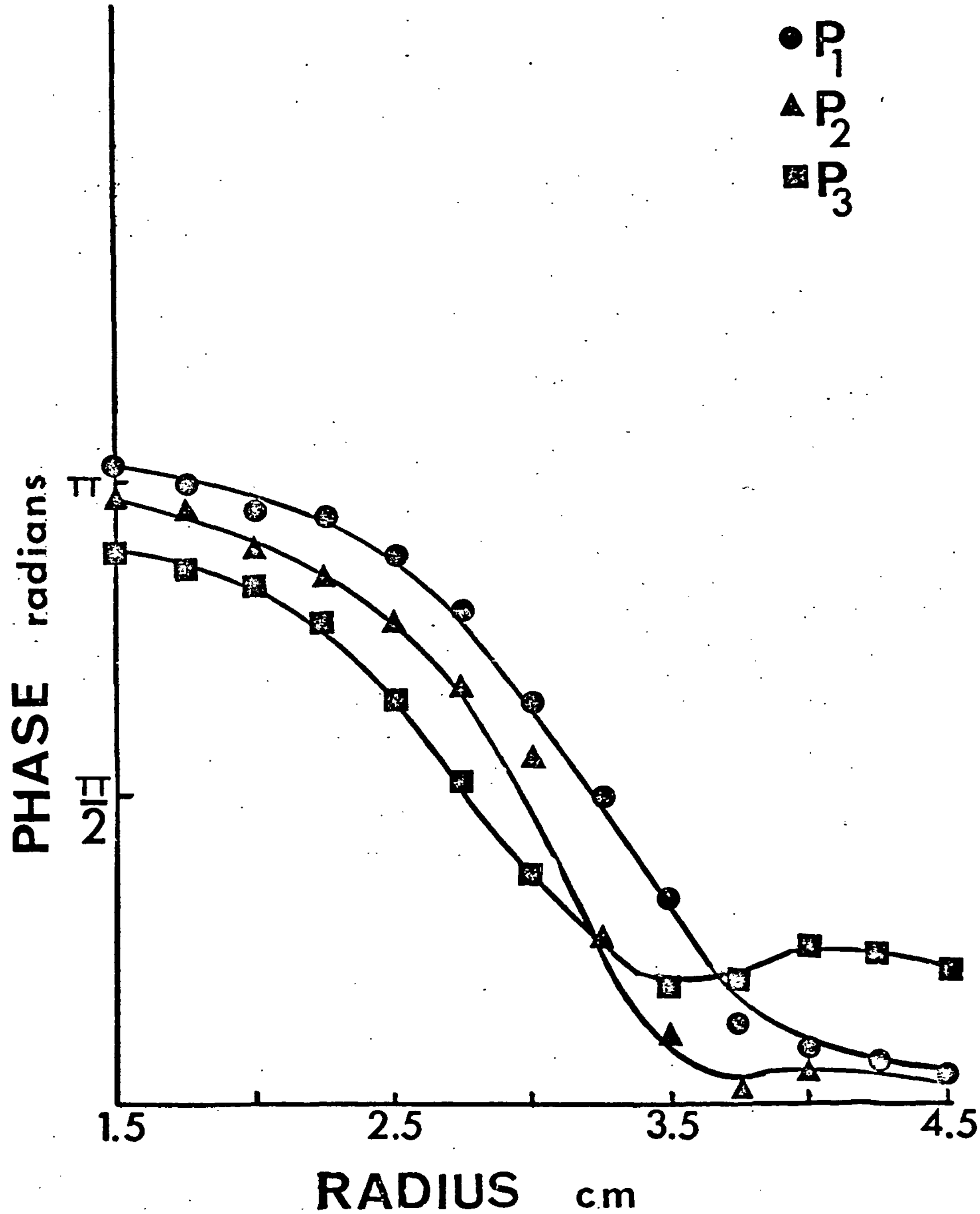

Figure 16

Phase difference between density and potential. Neutral pressure parameter.

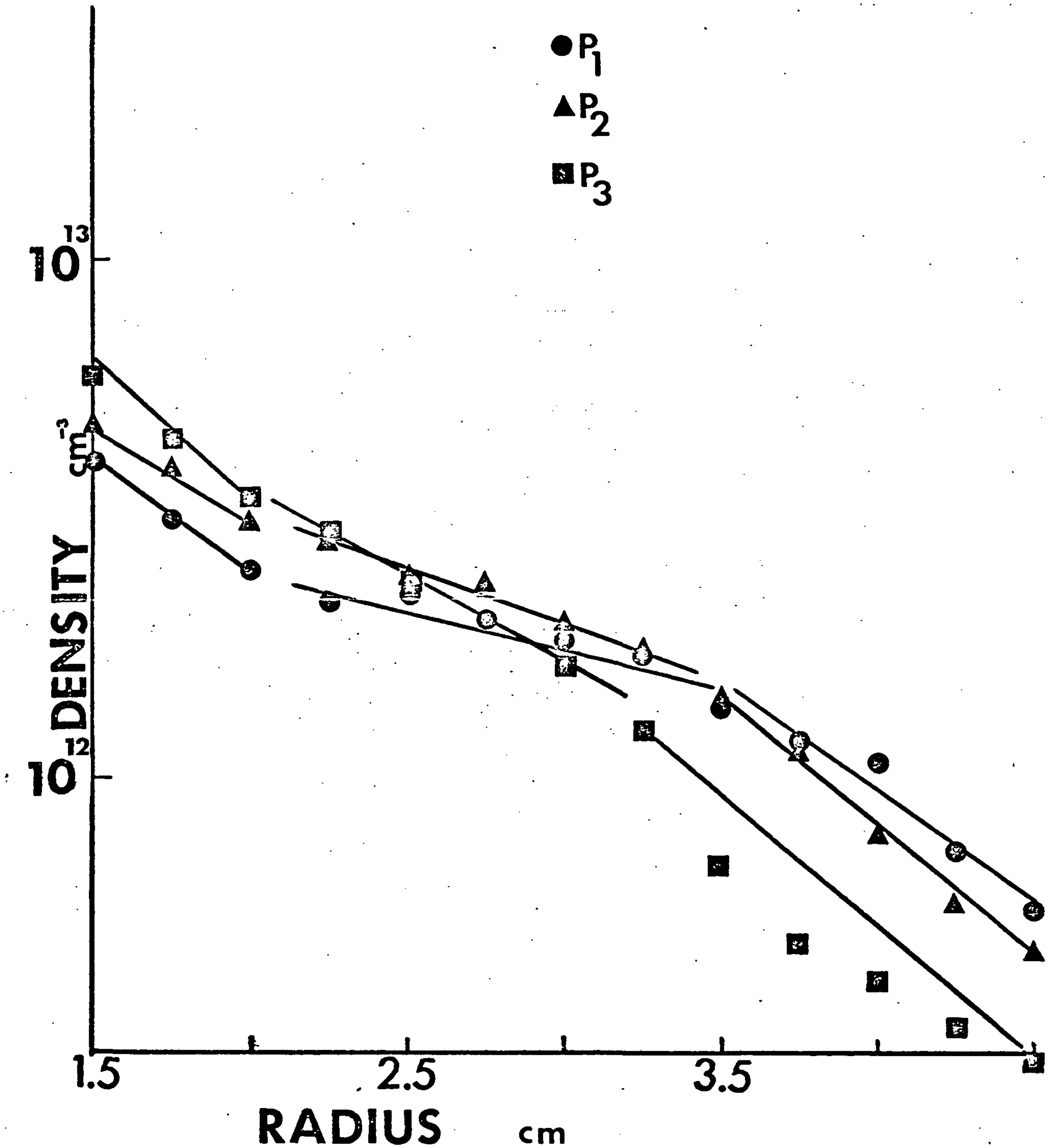

Figure 17

Ion density vs. radius Neutral pressure parameter.

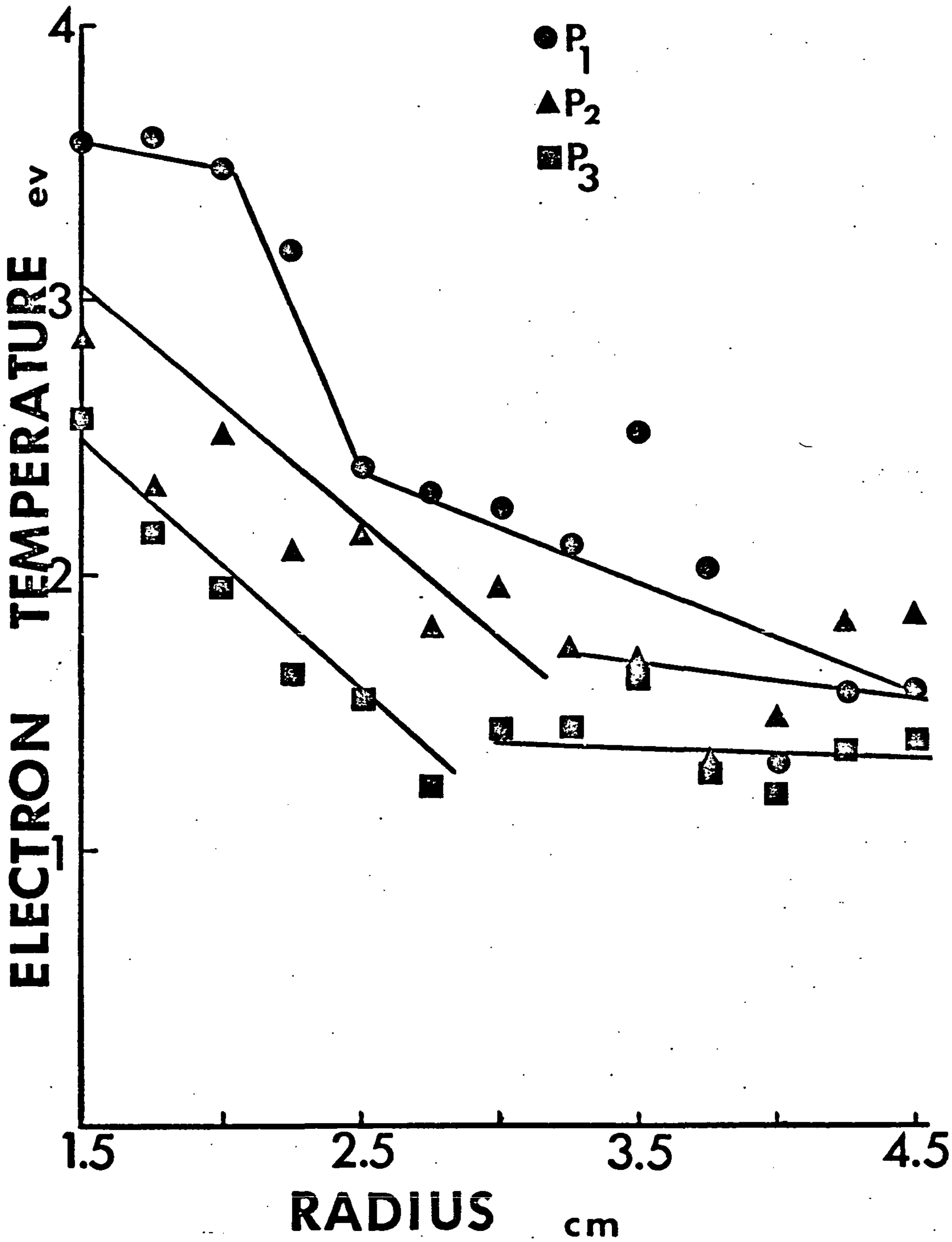

Figure 18

Electron temperature vs. radius Neutral pressure parameter.

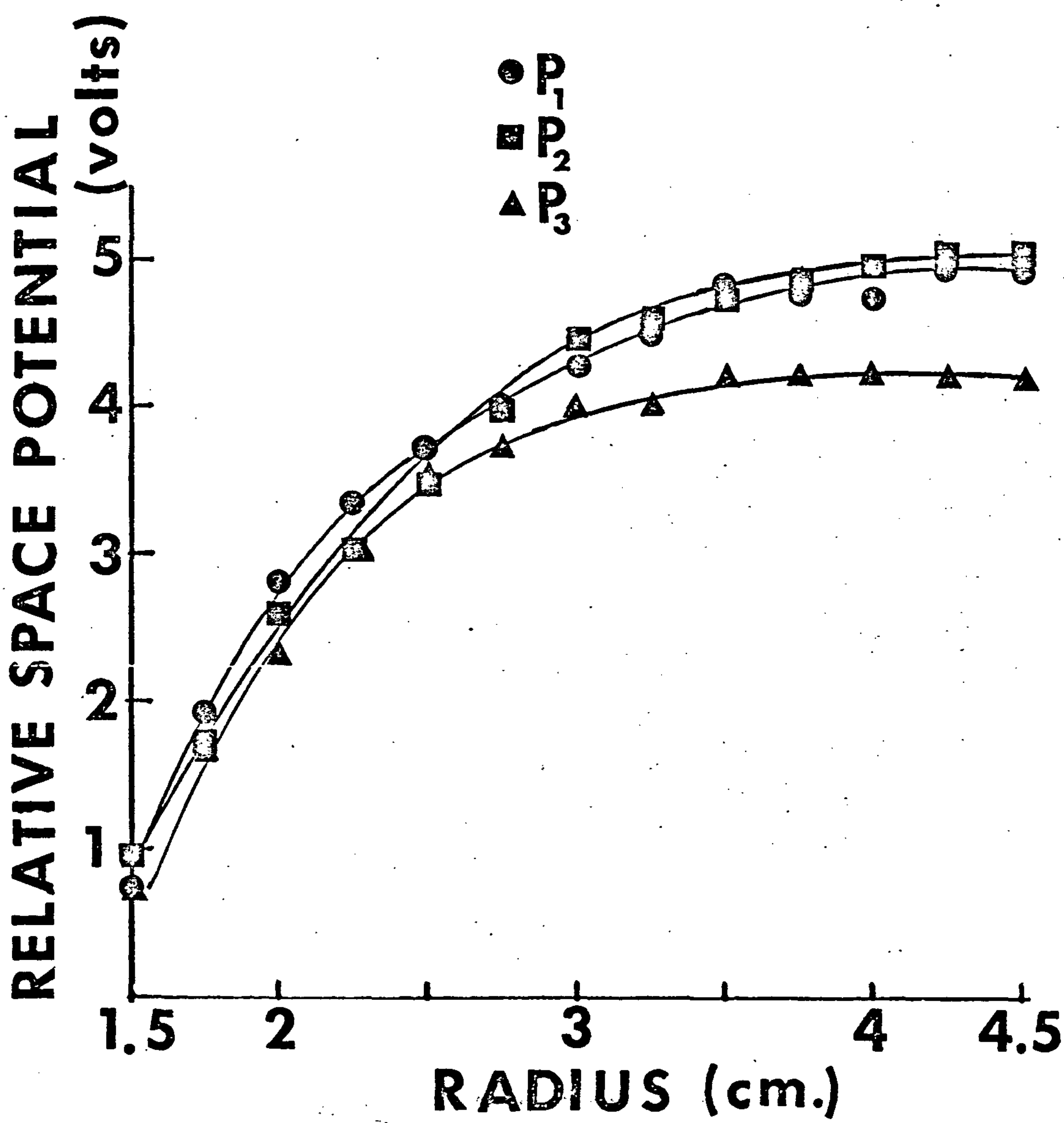

Figure 19

Relative Space potential vs. Radius. Neutral pressure parameter.

3) Variation of magnetic field

The steady state magnetic field was varied from 1.6 KG to 2.2 KG. At B_z=1.6 KG, the drift wave had a "soft" onset. Figure 20 shows the phase difference between ion density and potential for these magentic field values. It can be seen that the phase difference changed little at small radii, while there is a constant increase in the phase at large radii, for increasing field strengths. The density, temperature and potential gradients changed in a complex manner. The density gradients (Figure 21) were similar in slope and would not be expected to affect the phase significantly. The electron temperature (Figure 22) at r = 1.5 cm did not change much while the gradients changed significantly. The space potential variation is shown in Figure 23.

Figures 21 and 23 have variation in common. As the magnetic field was increased over the region of interest, the density gradient began at (B_1 = 1.6 KG) and eventually returned to (B_3 = 2.2 KG) a particular shape. The potential gradient underwent the same type of variation in its magnitude.

Changes in the values of ∇N_o, $\nabla \phi o$ and T were small as the externally controlled variables were changed. The magnitude of the phase difference was approximately the same for all data. It was close to 180^o for $r < 2.5$cm and $\sim 50^0$ for $r > 3.5$cm. These facts indicate that the phase difference was not very sensitive to our external controls. Hence, the character of the wave and its interaction with the plasma were not expected to vary to any great degree. The examination of the theory looked for variations in the phase difference, collision frequency and

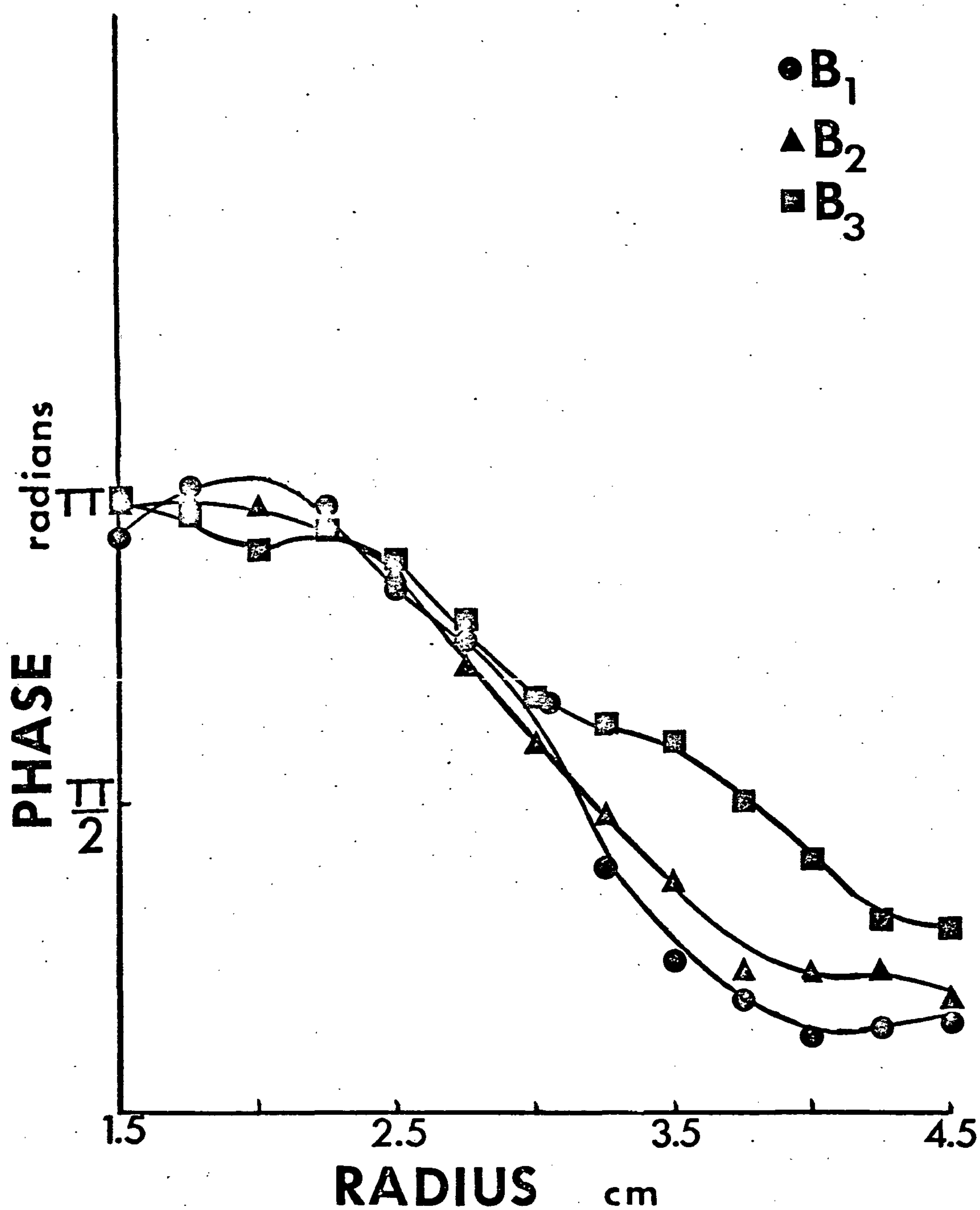

Figure 20

Phase difference between density and potential vs. radius. Magnetic field parameter.

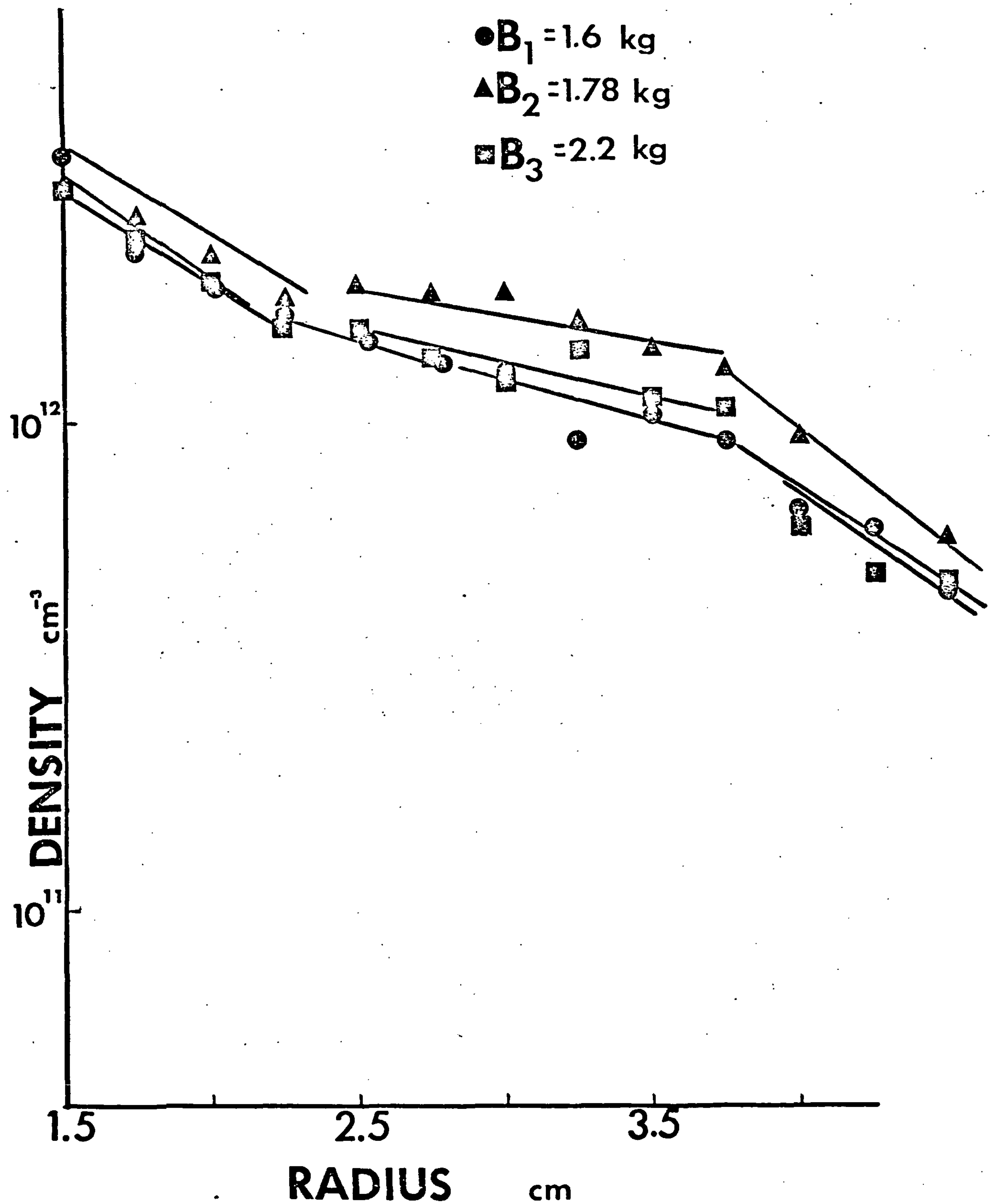

Figure 21

Ion density vs. radius. Magnetic field parameter.

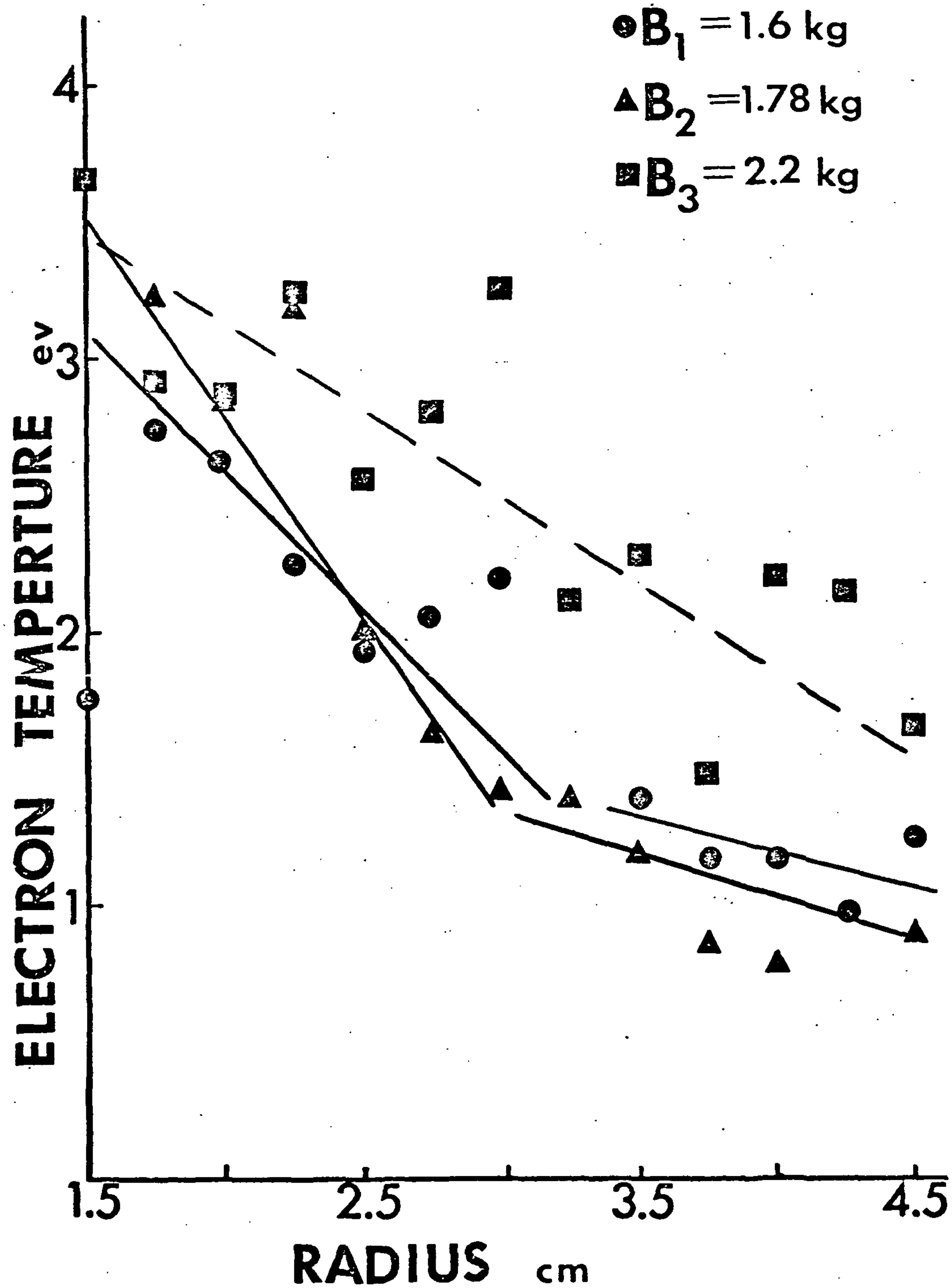

Figure 22

Electron temperature vs. radius.Magnetic field parameter.

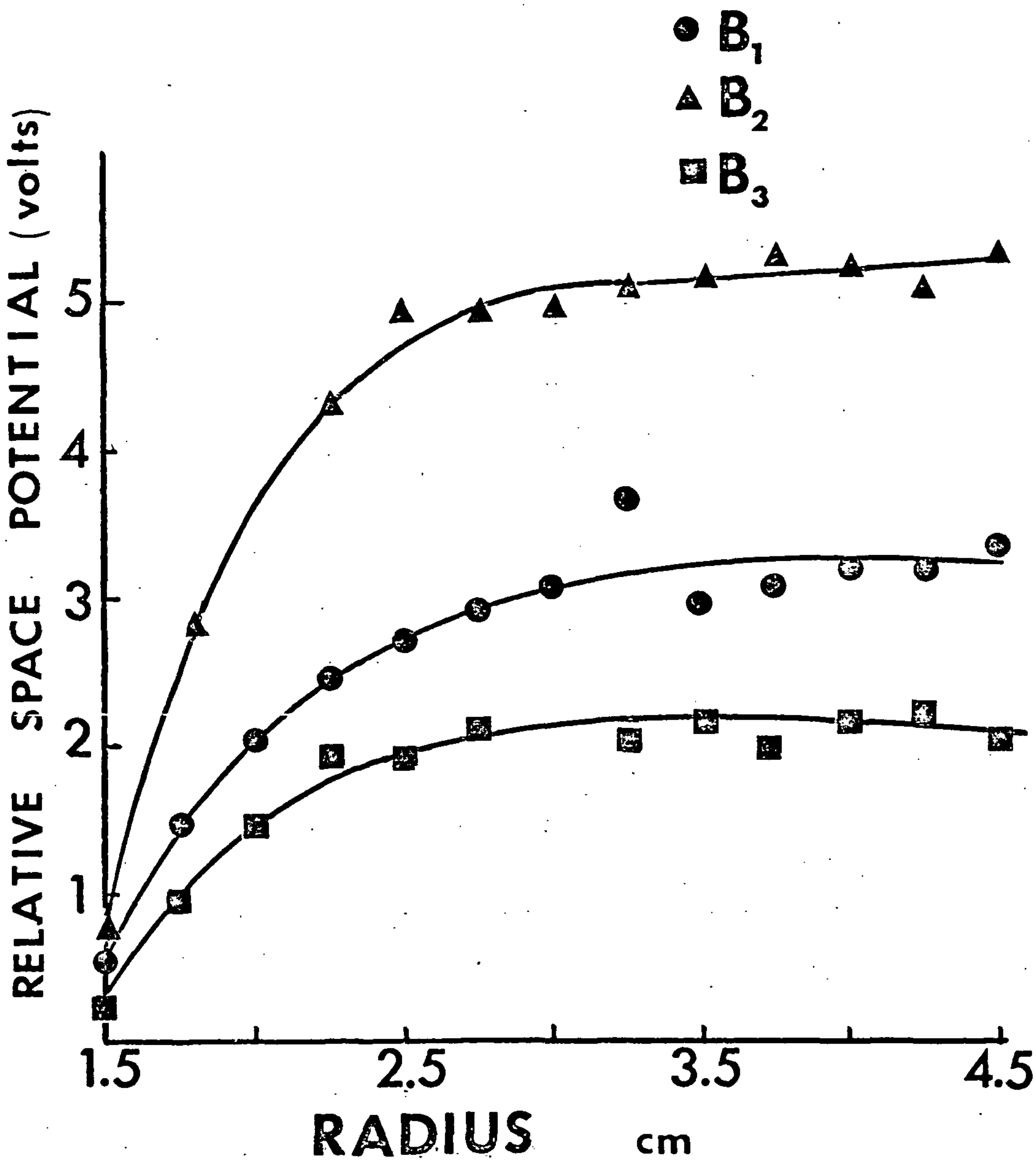

Figure 23

Relative Space potential vs. radius. Magnetic field parameter.

diffusion coefficient which would be consistent with the observed trends. From parts (1) and (2) of Section (B) we have noticed that variation of the pressure in the plasma affected the measured density gradient, and to some extent, the measured phase shift. Variation of this pressure was equivalent to variation of the collision frequencies. We expected ion-electron collisions to dominate close to the core ($r < 3$cm) and ion-neutral collisions to dominate at $r > 3$cm. In varying the gas flow rate we changed the condition of the plasma close to the core. The variation of neutral pressure affected the plasma conditions at large radii.

C. Theory

Linear theories for the drift wave have been developed for the quiescent cesiums plasmas (13), although drift waves occur in other devices similar to the Rensselaer arc (14). Chen (15) showed in a theoretical paper that the presence and growth of a wave depended on a phase shift between density and potential oscillations. Motley et.al. (16) and Aldridge et.al. (17) have reported phase shifts observed in drift waves. Motley reported phase shift calculations for a wave in a cesium plasma where temperature oscillations were included. The results indicated that floating and space potential have different phases with respect to the ion density. (i.e. one led and one lagged.) The difference between the space and floating potentials was 10-20° and not much larger than the error inherent in our phase sensitive detector. We chose initially to develop a theory neglecting temperature oscillations.

We use the ion fluid equations with the following assumptions. The mode is a flute mode and $k_r a \ll 1$ where a is a radial scale length for a gradient of ion density or potential and k_r is a radial wavelength. The electric field is electrostatic and $\omega \ll \omega_{ci}$ where ω is the wave frequency and ω_{ci} is the ion cyclotron frequency; also $T_i \ll T_e$. Assumption of the localization condition enables us to ignore the particle source term in the ion continuity equation. We neglect the term $(\mathbb{V}\cdot\nabla\mathbb{V})$ in the ion momentum equation because spatial derivatives of the velocity across the radial position of the wave are insignificant.

Our initial equations are

$$\frac{\partial N_i}{\partial t} + \nabla\cdot(N_i \mathbb{V}_i) = 0 \tag{III-1}$$

$$m_i \frac{d\mathbb{V}_i}{dt} = -e\nabla\phi + e\mathbb{V}_i \times \mathbb{B} - kT_i \frac{\nabla N}{N} - m_i \mathbb{V}_i \nu_i \tag{III-2}$$

All symbols are standard and ν_i is the effective ion collision frequency $\nu_i = \nu_{iN} + \nu_{iE}$ where N refers to neutrals and E to electrons. We would expect that ν_{iE} is important close to the core and that ν_{iN} is important at large radii. We assume ϕ and N_i are perturbed in the form $x = x_0 + x_1$ where $x_1 \ll x_0$ and $x_1 = |x_1| \, e^{ik_y\phi - i\omega t}$ and x is either N_i or ϕ_i. Combining (1) and (2) with the perturbations we obtain

$$-i\omega N_i + N_o A \left(-\mu_i L\nabla^2\phi_1 - D_i \frac{L}{N_o} \nabla^2 N_i \right)$$

$$+ AL \left(-\mu_i \left(\nabla_x \phi_1 \nabla_x N_o + \nabla_z\phi_1 \nabla_z N_o\right) - \frac{D_i}{N_o} \left(\nabla_x N_i \nabla_x N_o + \nabla_z N_i \nabla_z N_o \right) \right)$$

$$+ A \left(\frac{\omega_{ci}}{\nu_i}\right) \left(-e \nabla_x N_o \nabla_y \phi_1 - \frac{D_i}{N_o} \nabla_x N_o \nabla_y N_1 \right)$$

$$+ H\left(-\mu_i \left(\nabla_x\phi_o\nabla_x N_1 + \nabla_z\phi_o\nabla_z N_1\right) - \frac{D_i}{N_o} \left(\nabla_x N_o\nabla_x N_1 + \nabla_z N_o\nabla_z N_1\right)\right)$$

$$+ H \left(\frac{\omega_{ci}}{\nu_i}\right) \left(e \nabla_y N_1 \nabla_x \phi_o + \frac{D_i}{N_o} \nabla_y N_1 \nabla_x N_o \right) = 0 \tag{III-3}$$

$$\text{where } \frac{1}{A} = (1 - i\omega\tau_i)^2 + \omega_{ci}^2\tau_i^2 = L^2 + \omega_{ci}^2\tau_i^2 \qquad \text{(III-4)}$$

$$\frac{1}{H} = 1 + \omega_{ci}^2\tau_i^2 = 1 + \beta^2 \qquad \text{(III-5)}$$

D_i = Field free diffusion coefficient

μ_i = Field free ion mobility

This equation is more general than our final result because it still contains axial gradients which will be included in future work. Equation (3) was combined with the previously stated assumptions. The result relates ion density and potential fluctuations

$$\frac{N_i}{N_o}\left\{(ALD_i\ k_y^2) - ik_y\left(\omega + A V_d\beta^2\left(\frac{T_i}{T_e}\right) - H\beta^2\left(\frac{\phi_o}{B} + V_d\left(\frac{T_i}{T_e}\right)\right)\right)\right\}$$

$$= \frac{e\phi_1}{kT_e}\left\{- AL\,\beta\left(\frac{kT_e}{eB}\right) k_y^2 + i A \beta^2 V_d k_y^2\right\} \qquad \text{(III-6)}$$

At marginal stability of a drift wave ω is purely real because the growth rate, Im (ω), is zero. It is of interest to note that at the maximum amplitude of the wave $\frac{N_{e1}}{N_o} = \frac{e\phi_i}{kT_e}$ was experimentally true. This leads to a local dispersion relation for the wave

$$(ALD_i\ k_y^2) - ik_y\left(\omega + A\beta^2V_d\left(\frac{T_i}{T_e}\right) - H\beta^2\left(\frac{\phi_o}{B} + V_d\frac{T_i}{T_e}\right)\right) = iA\beta^2V_dk_y - AL\beta\,\frac{kT_e}{eB})k_y$$

(III-7)

In this report we concern ourselves only with the calculation of the density-potential phase difference. Since $\omega \ll \omega_{ci}$ is assumed we have $L \approx 1$ and $A \approx H$. Then equation (III-6) becomes linear in ω. In this form the dominant term in the dispersion relation is $\omega \approx k_y V_d$ (18) where V_d is the ion drift velocity

$$V_d = -\frac{kT_e}{eB}\frac{\nabla N_o}{N_o} + \frac{\nabla \phi_o}{B} \tag{III-8}$$

from Chen (19). We use this drift velocity to correctly account for the strong potential gradient that exists in our plasma.

Equation (III-6) was analyzed in a straight forward manner. It may be written as

$$\frac{N1}{N_o}(A + i B) = \frac{e\phi_1}{kT_e}(C + i D) \tag{III-9}$$

where A and B are the real and imaginary parts of the left hand side of equation (4) and C and D correspond to the same for the right hand side. Using $\frac{N_1}{N_o} = \frac{e\phi_1}{kT_e} F e^{i\xi}$, where F is the ratio of the amplitudes $\frac{N_1/N_o}{e\phi_1/kT_e}$ and ξ is the phase angle, we obtain in terms of plasma parameters

$$\xi = \tan^{-1}\left[\frac{k_y\left(V_d D_{i\perp} - V_d\left(\frac{kT_e}{eB}\right) + \left(\frac{\beta^2}{1+\beta^2}\right)\left(\frac{kT_e}{eB}\right)\left(\frac{\nabla\phi_o}{B}\right)\right)}{-D_i^2 k_y^2\left(\frac{kT_e}{eB}\right) - V_d\left(V_d - \left(\frac{\beta^2}{1+\beta^2}\right)\frac{\nabla\phi_o}{B}\right)}\right] \tag{III-10}$$

$$F = \left[\frac{\frac{\beta^2}{(1+\beta^2)^2}\left(V_d^2\beta^2 + \left(\frac{kT_e}{eB}\right)^2 k_y^2\right)}{D_{i\perp}^2 k_y^2 + \left(V_d - \left(\frac{\beta^2}{1+\beta}\right)\frac{\nabla\phi_o}{B}\right)^2}\right]^{1/2} \tag{III-11}$$

$$\text{where} \quad D_{i\perp} = \frac{D_i}{1+\beta^2} \tag{III-12}$$

Equations (10) and (11) were those obtained from linear theory. Eq. 10 was examined in more detail and the results are reported in the next section. The effect of the collision frequency ν_i is contained in

$\beta = \omega_{ci}\tau_i$. Solving equation (10) for β led to a cubic equation in β. We chose then to pick β and try to predict the phase difference with Eq. (11).

D) Comparison of Theory and Equipment

Equation (11) was solved by a computer program using values of arc parameters taken from experimental data. $\nabla N_o, \nabla \phi_o$, T_e and V_d are obtained either directly by measurement or by evaluation from probe curves measured simultaneously with experimental phase difference measurements. The only parameter not specified in this manner was ν_i. This was used as a variable parameter to obtain the best fit between theory and experiment. In the fitting operation it was found that the convention $|k_y = - k_y$ was required. This was equivalent to measuring the direction of the wave. In our analysis this meant that the wave would be traveling in the ion diamagnetic direction. This was consistent with our experimental results if plasma rotation is taken into account. The plasma rotated in the electron diamagnetic direction direction, Doppler shifting the observed frequency of the wave so that the measured direction of propagation is the electron diamagnetic direction.

The standard drift wave conditions were the first to be analyzed. Figures 13, 14 and 15 were used to obtain the values of ∇N_o, $\nabla \phi_o$ and T_e. ν_i in units of ω_{ci} is used to fit Eq. (11) to the experimental phase difference curves. Equation (11) is plotted in Figure 24 as a function of $\alpha = 1/\beta$. Figure 24 is in fair agreement with the measured phase differences, Figures 12, 16 and 20. At radii $r < 3$cm., the phase $> 90^o$ and at radii $r > 3$ cm., $< 90^o$. We picked a value of α for each radial range, α_1 essentially representing ν_{iE} ($r < 3$ cm) and α_2 for $r > 3$ cm where ν_i was essentially ν_{iN}. These curves in Fig. 24* enabled us to estimate values for α to fit the experimental phase difference curves. Some values of α ($\alpha = 5,10$) did not give continuous smooth curves across the region 2.5 cm $\leq r \leq 3$ cm. Because of this we did not expect close fits between theory and experiment in this region. A model of the phase shift with only two values for the collision frequency is not physically realizable. We did this initially to test the fit of the model.

Figure 25 shows three curves. An experimental curve and two theoretical curves; one with $\alpha_1 = \alpha_2 = 1$, and a second with $\alpha_1 = .1$, $\alpha_2 = 3$. A constant collision frequency does not give correct results, but on choosing two values for α, we obtain better correspondence. Physically, this can be interpreted as a change from a region where ion-electron collisions dominate, to one where ion-neutral collisions dominate.

The resultant collision frequencies and diffusion coefficients are shown in Figures 26 and 27. Collision frequencies are usually $\alpha_1 < 1$ $\alpha_2 > 1$. The diffusion coefficient shows some enhancement at $r > 3$ cm.

a) Variation of Flow Rate

The experimental and theoretical curves* for the phase difference are shown in Figures 25, 28 and 29. Agreement is good at large, $r > 3.5$ cm, and small radii, $r < 2.5$ cm. Data points in the region where the phase difference is $\approx 90^{\circ}$ were more difficult to fit due to the argument of equation (11) approaching $\pm \infty$. This is shown by the choice of the variable parameter ν_i, shown in Figure 30. The collision frequency shows enhancement at this point. Note that the enhancement takes place at the same radial point, $r = 2.5$ cm, for each curve. While the amplitude of the

---

* From Eq. 11

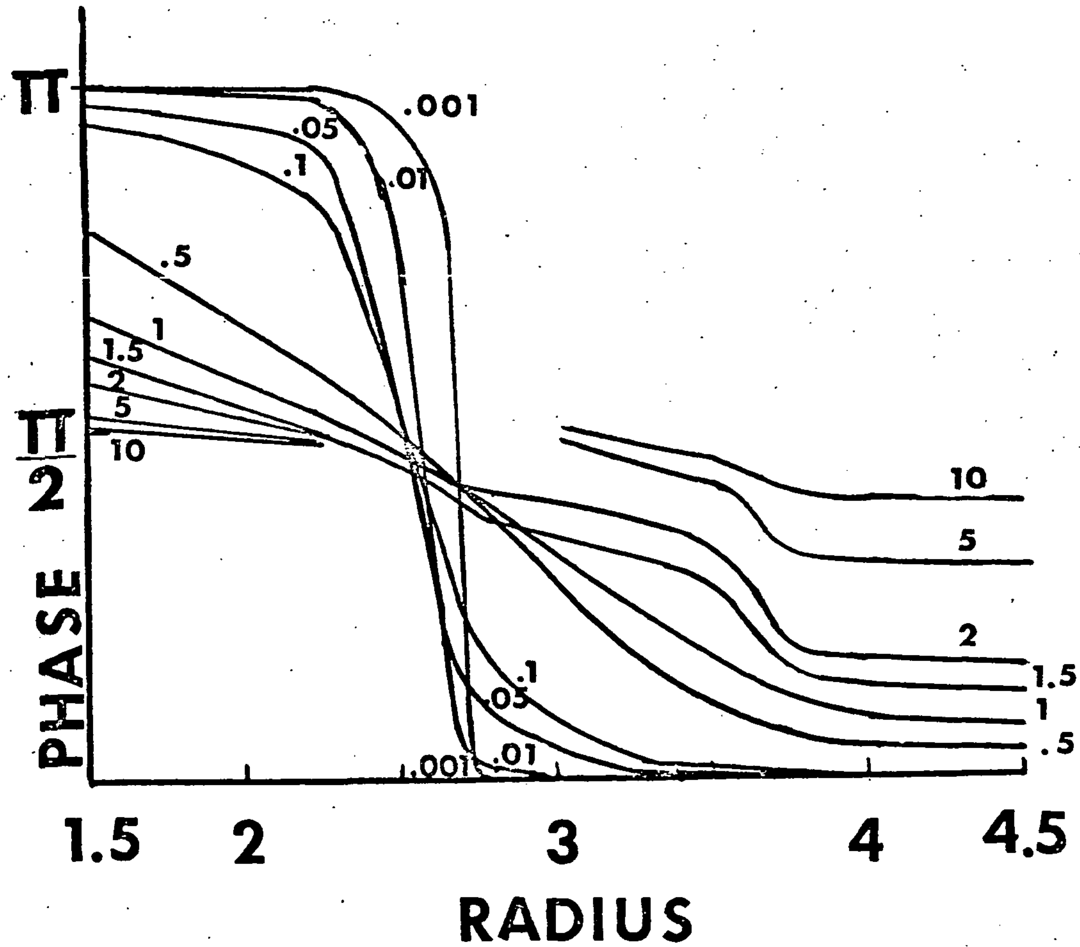

Figure 24

Phase vs. radius calculated from eq. (III-11). $\beta = \omega_{ci}\tau_i$ parameter. Values on (24) are α. $\alpha = 1/\beta$

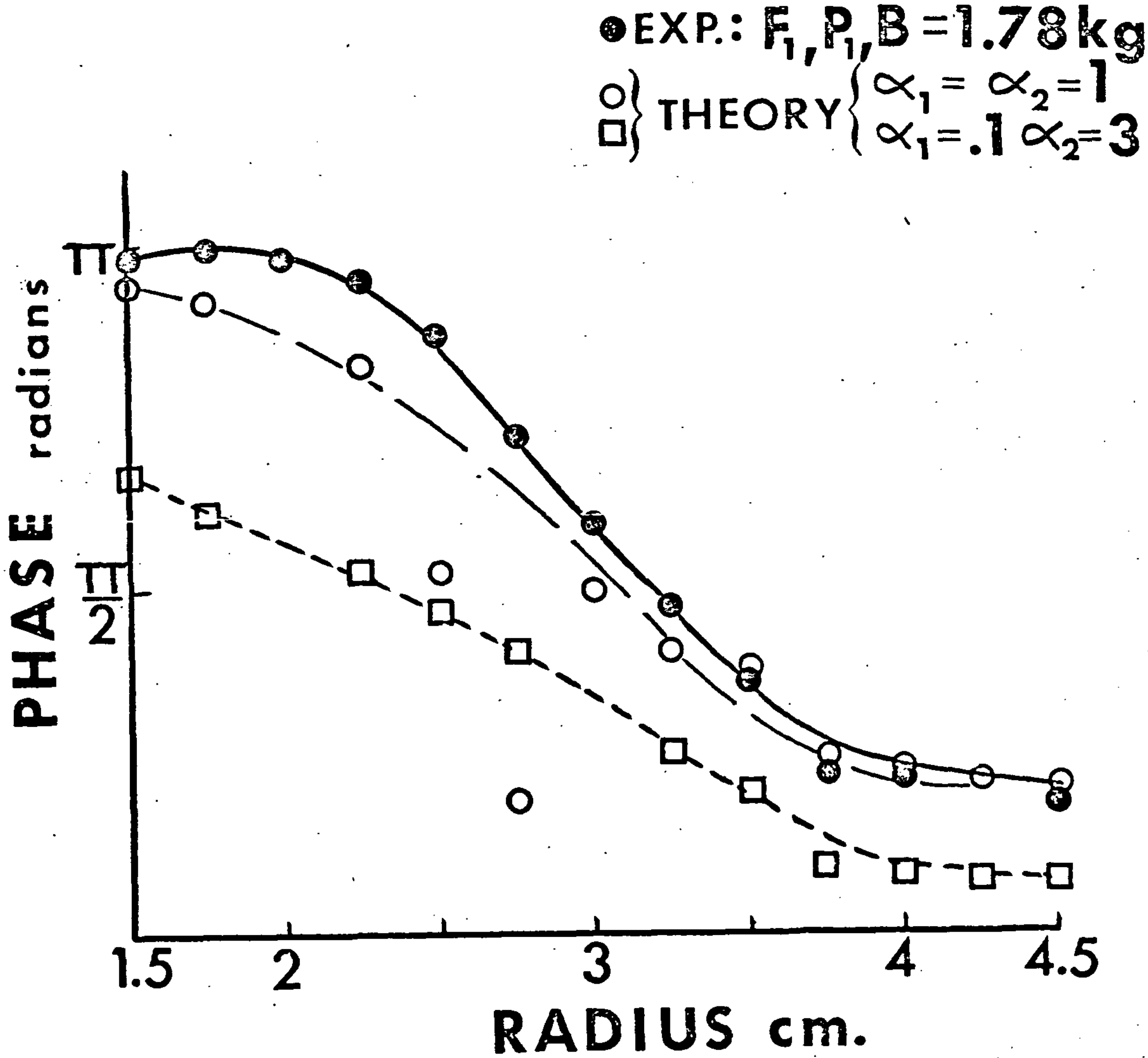

Figure 25

Calculated phase difference between density and potential vs. radius
Standard drift wave conditions α_1: $r < 3$ cm, α_2: $r \geq 3$ cm.

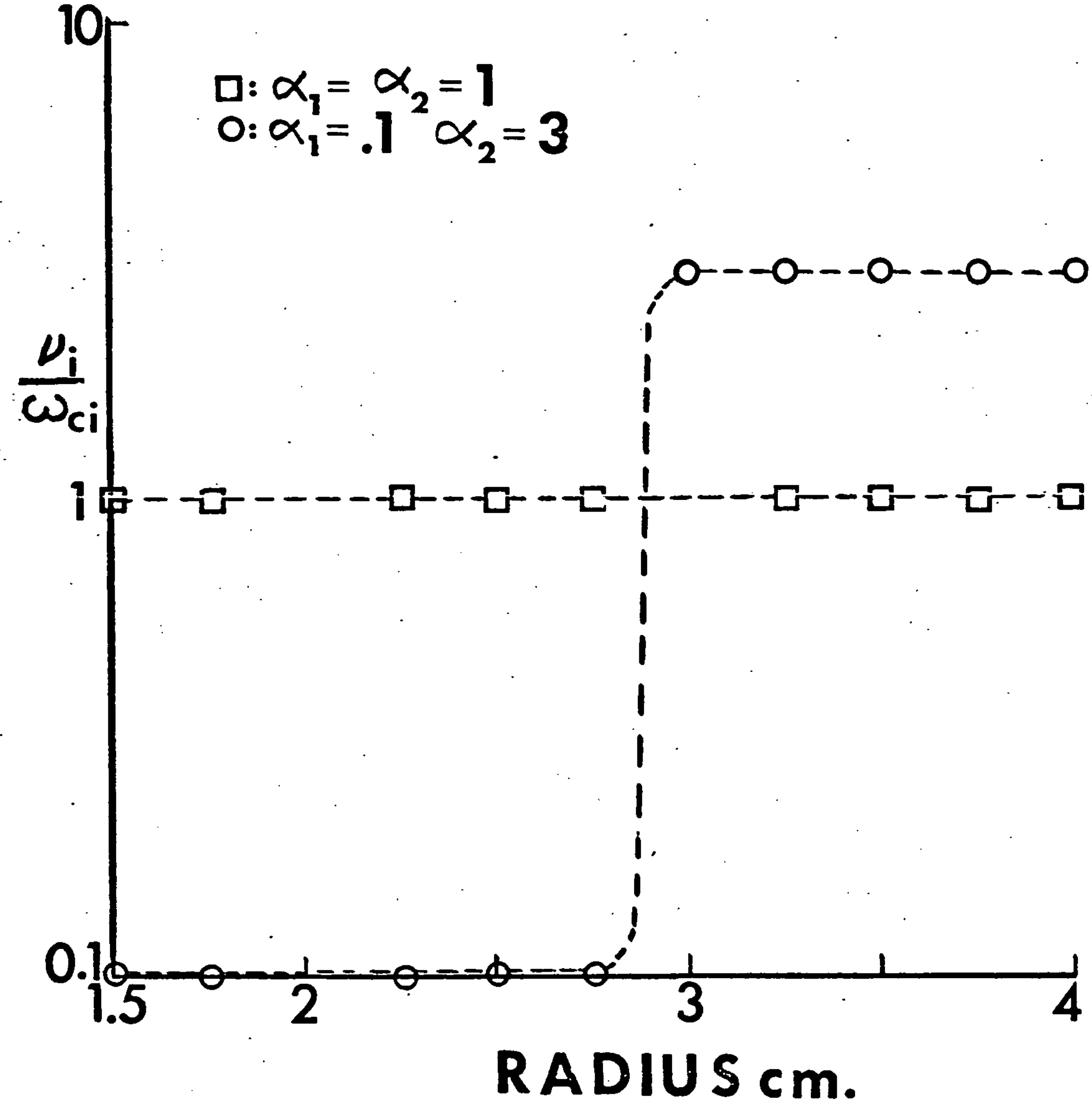

Figure 26

Collision frequency (in units of ω_{ci}) vs. radius. Standard drift wave conditions

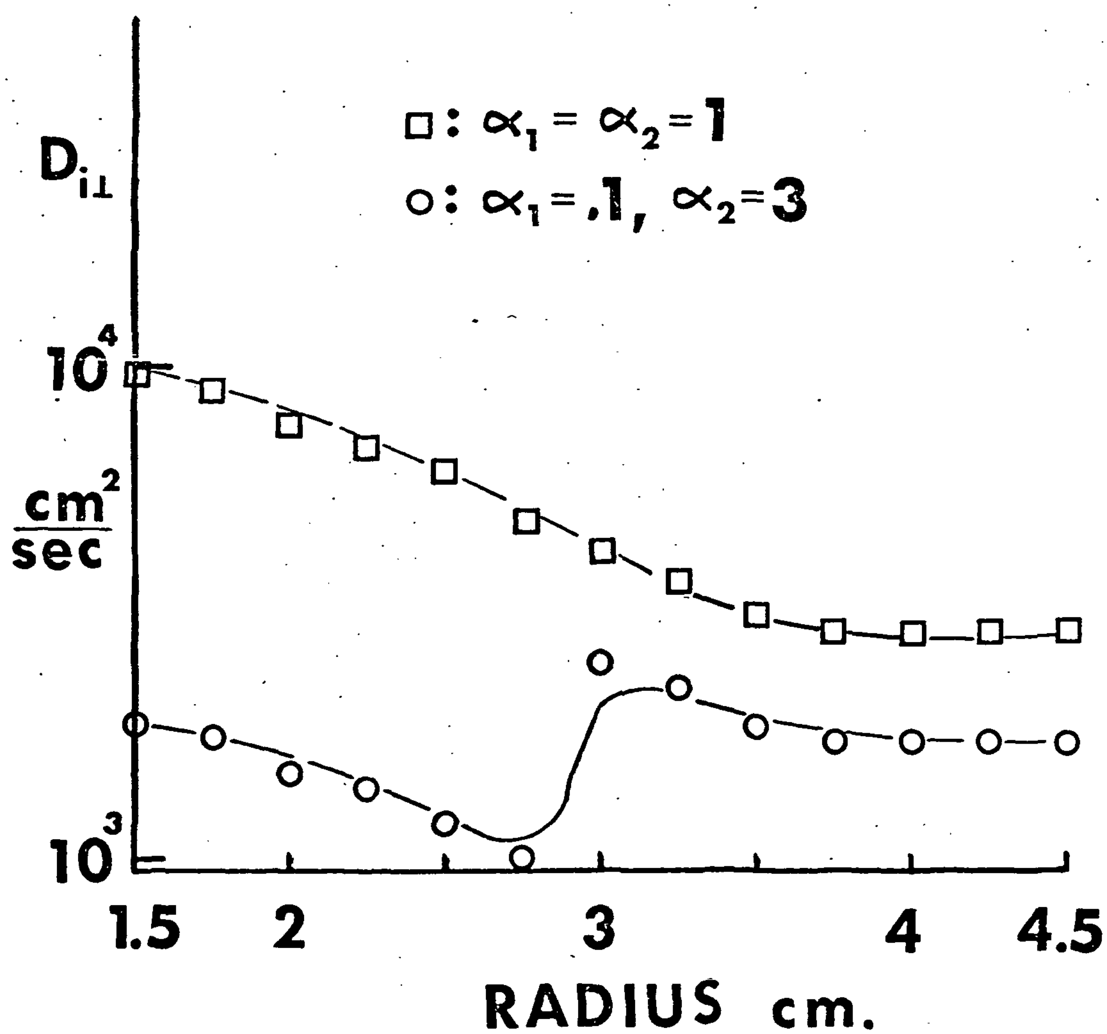

Figure 27

Diffusion coefficient vs. radius. Calculated using $T_i = .1 \times T_e$. Standard drift wave conditions

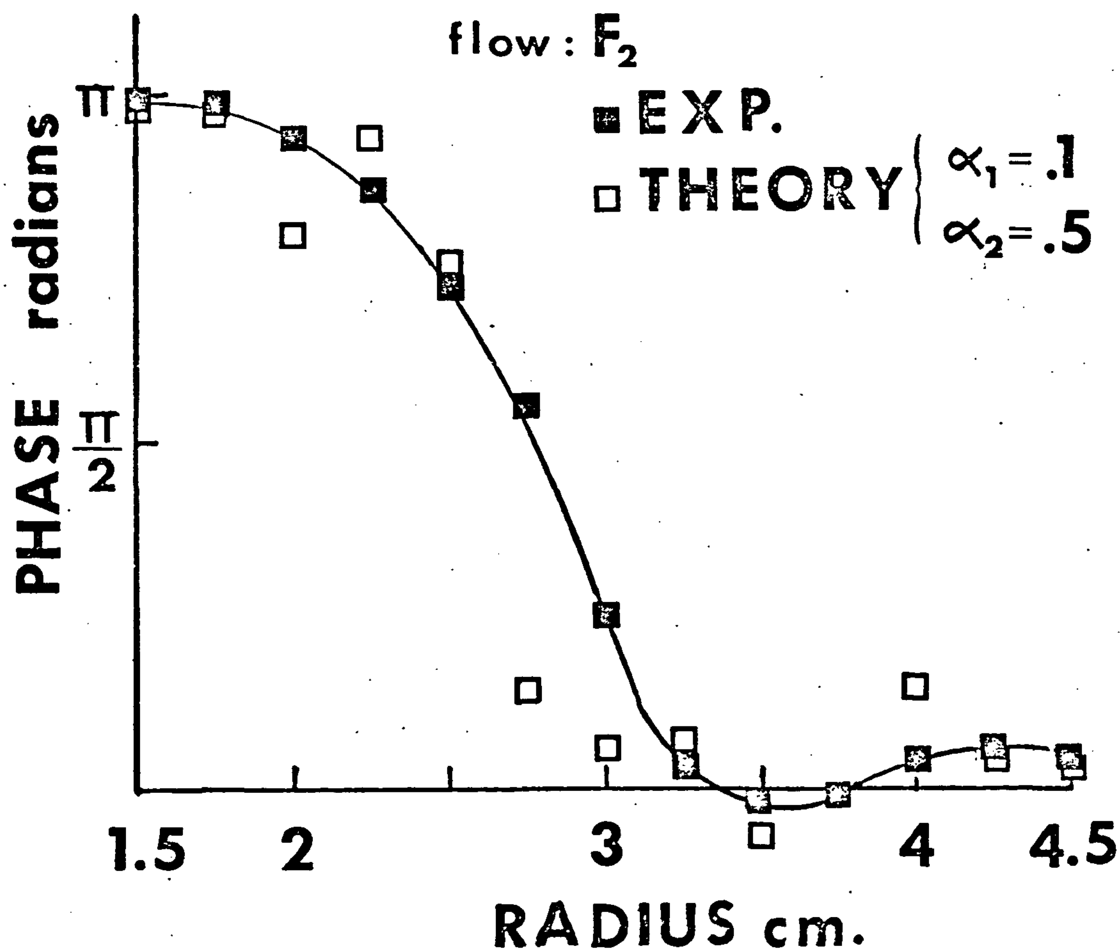

Figure 28

Phase vs. radius calculated from (III-11) α_1; $r < 3$ cm, α_2; $r \geq 3$ cm

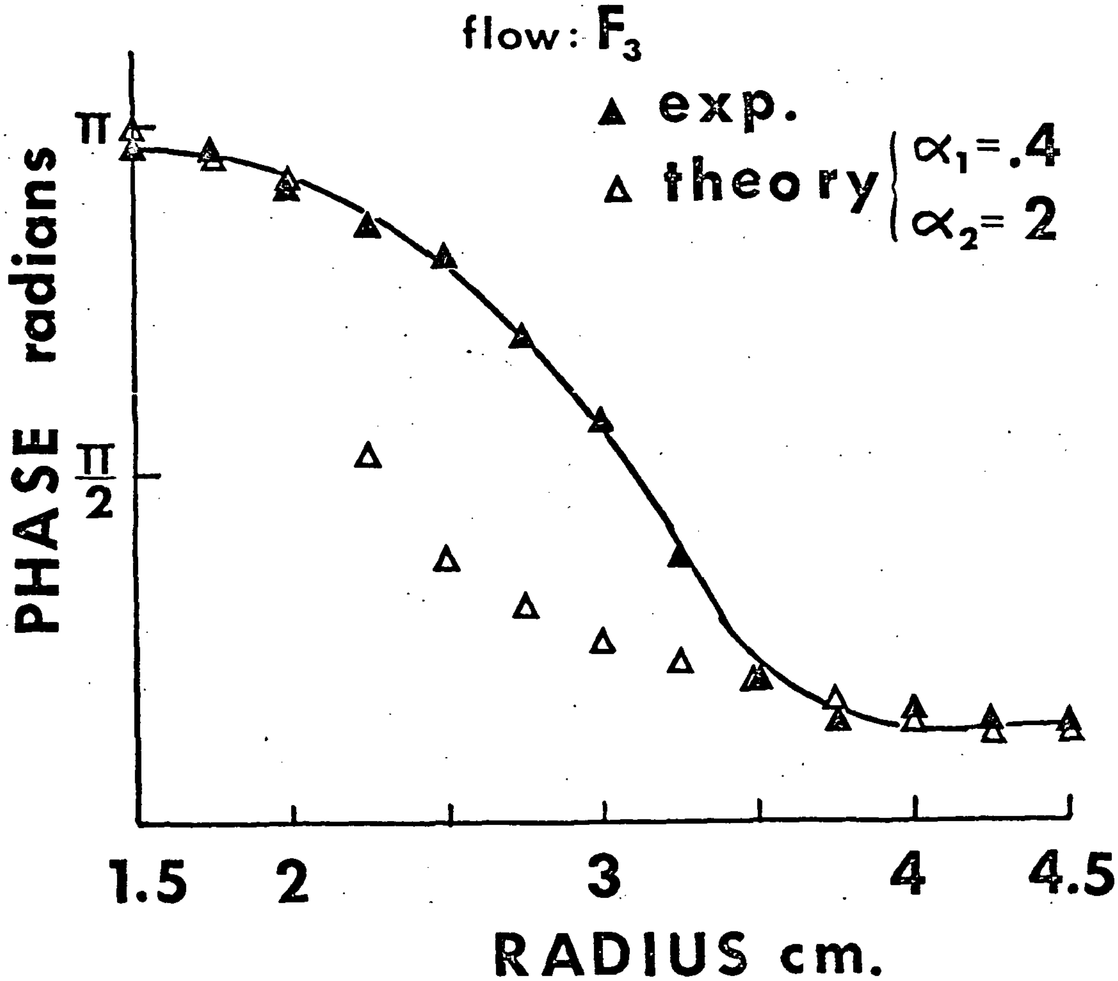

Figure 29

Phase vs. radius calculated from (III-11) α_1; $r < 3$ cm, α_2; $r \geq 3$ cm. Flow rate parameter.

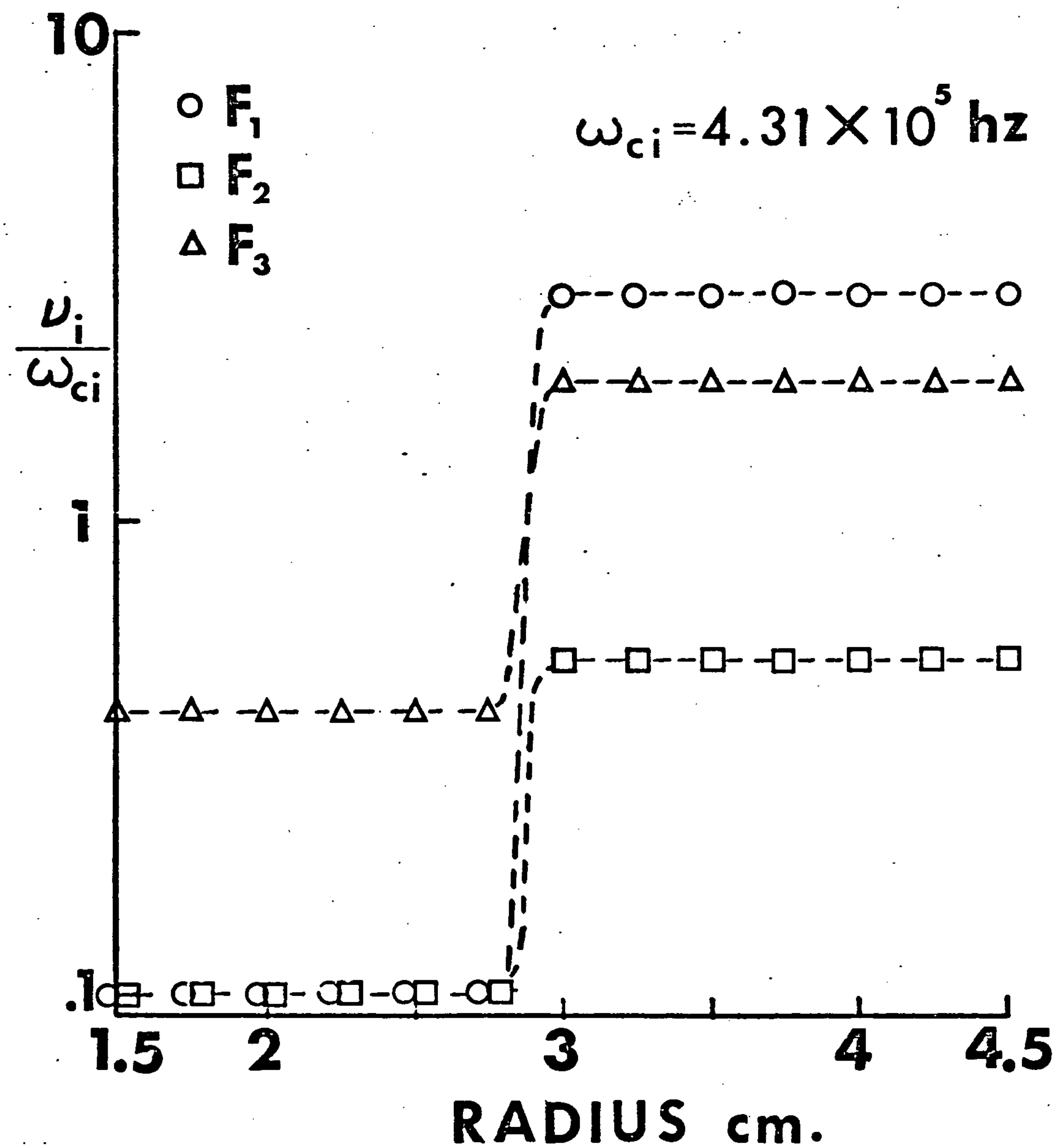

Figure 30

Collision frequency vs. radius. Flow rate parameter.

wave was affected by the variation in flow rate, its interaction with the plasma in a radial direction was not. Enhancement of the diffusion coefficient, Figure 31, occured at the same radial regions. Hence axial drifts influence the growth of the wave close to the core but do not influence the radial interaction of the wave with the plasma.

b) Variation of Neutral Pressure

Experimental and theoretical curves for the phase difference are shown in Figures 32, 33 and 34. Improved fits were found at all radii. Figure 35 shows the variation of ν_i as a function of radius and neutral pressure. The increased pressure has the effect of reducing the amplitude of the wave. Enhancement of the collision frequencies begins at smaller radii for higher neutral pressure. It would be expected that the effects of neutrals would be to change the collision frequency at a different position in the plasma. The different mechanism for increasing the neutral pressure, as contrasted to variation of flow rate, shows up in the enhanced ion collision frequency at smaller radii. In part (a), the increased flow rate balanced out the neutral pressure increase and enhancement of ν_i occured at the same radial point. The flow rate must be taken into account as as axial effect, while the increased pressure will be a radial neutral gradient effect. The diffusion coefficient also varied in the expected manner. Enhanced diffusion coefficients occured at smaller radii as neutral pressure increased (Figure 36).

c) Magnetic Field Variations

Figure 25 was the phase difference when the magnetic field was at its standard value B_2 = 1.78 KG. This is to be compared with Figure 37 when the magnetic field was 1.6 KG. A reasonable fit was obtained with a similar

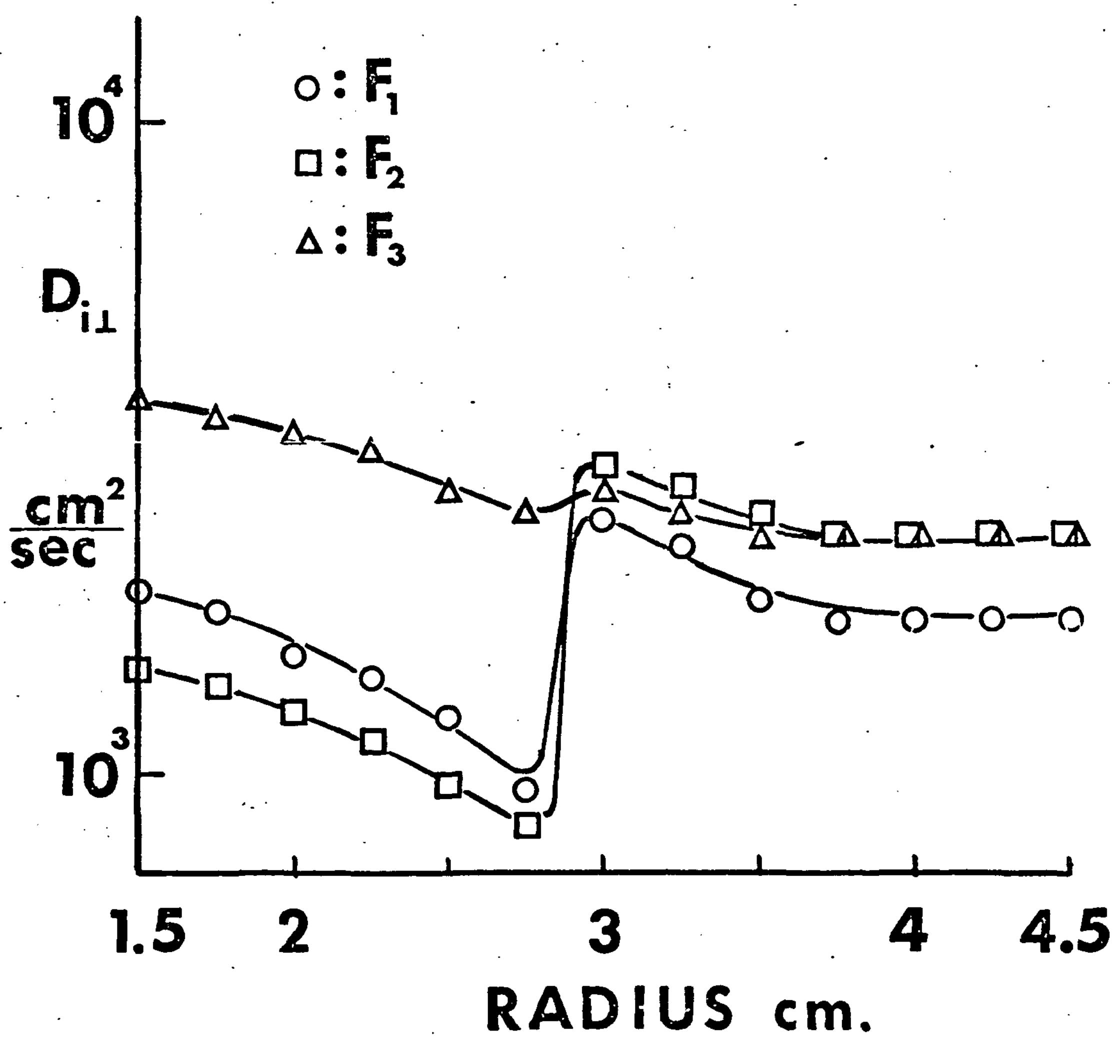

Figure 31

Diffusion coefficient vs. radius. Calculated as in Fig. 27. Flow rate parameter.

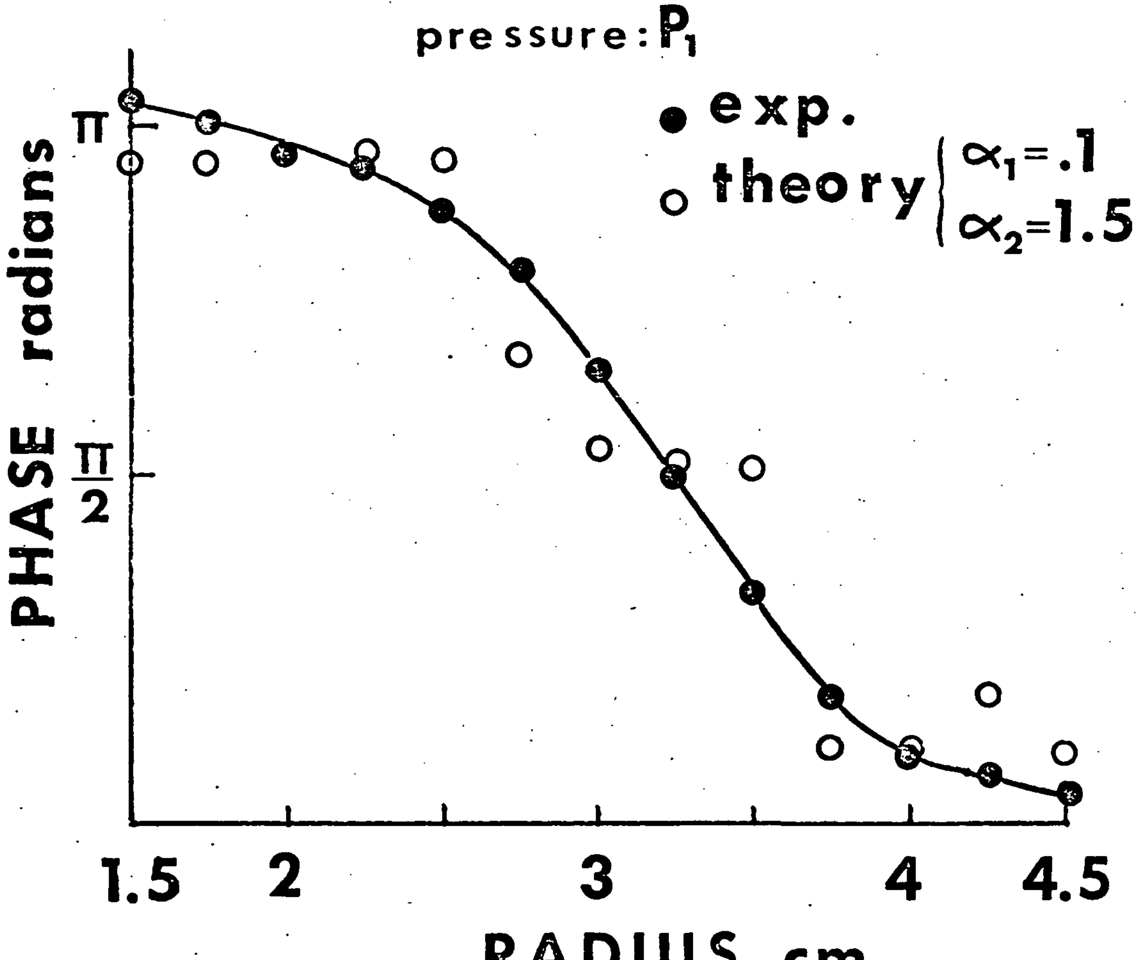

Figure 32

Phase vs. radius. Calculated from (III-11) α_1; $r \leq 2.5$ cm, α_2; $r > 2.5$ cm. Neutral pressure parameter.

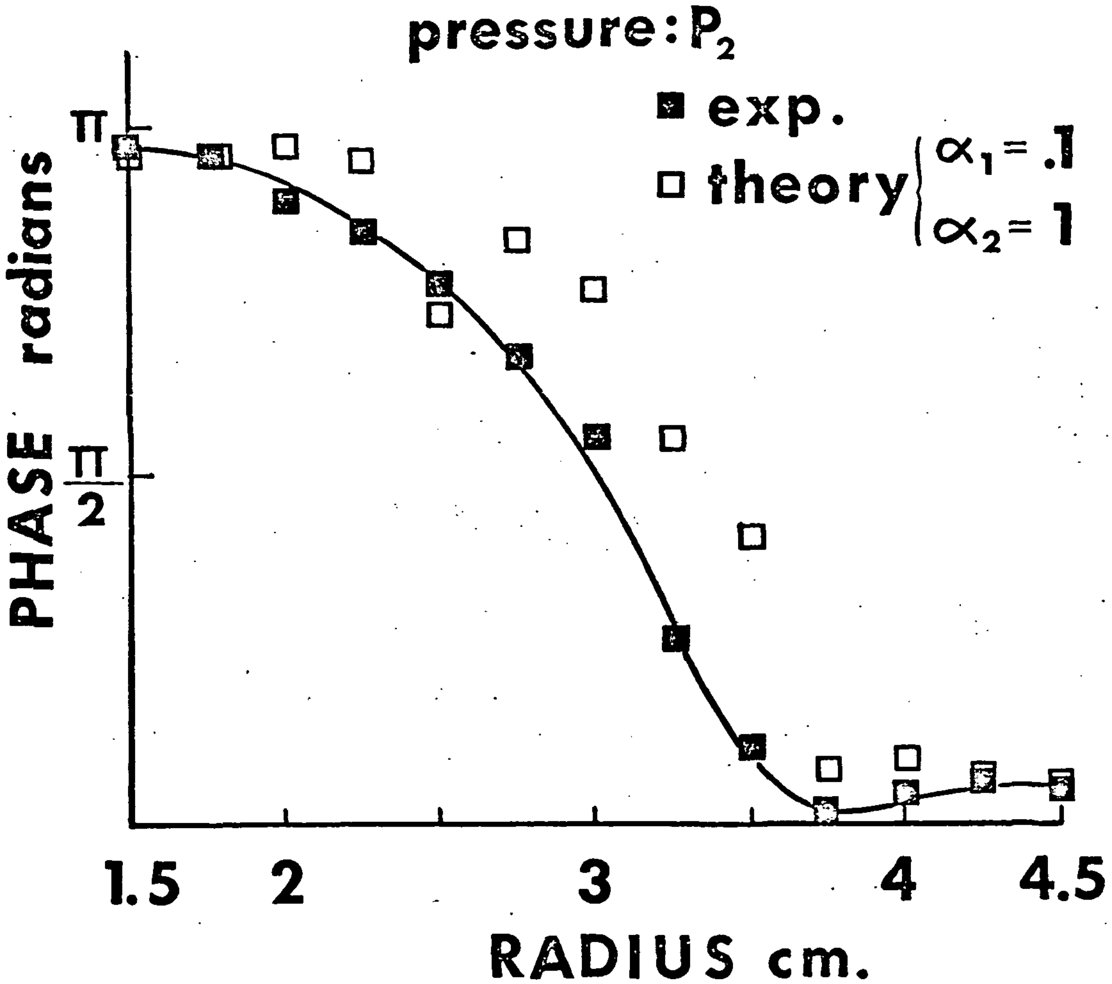

Figure 33

Phase vs. radius Calculated from (III-11) α_1; $r < 2.5$ cm, α_2; $r \geq 2.5$ cm. Neutral pressure parameter

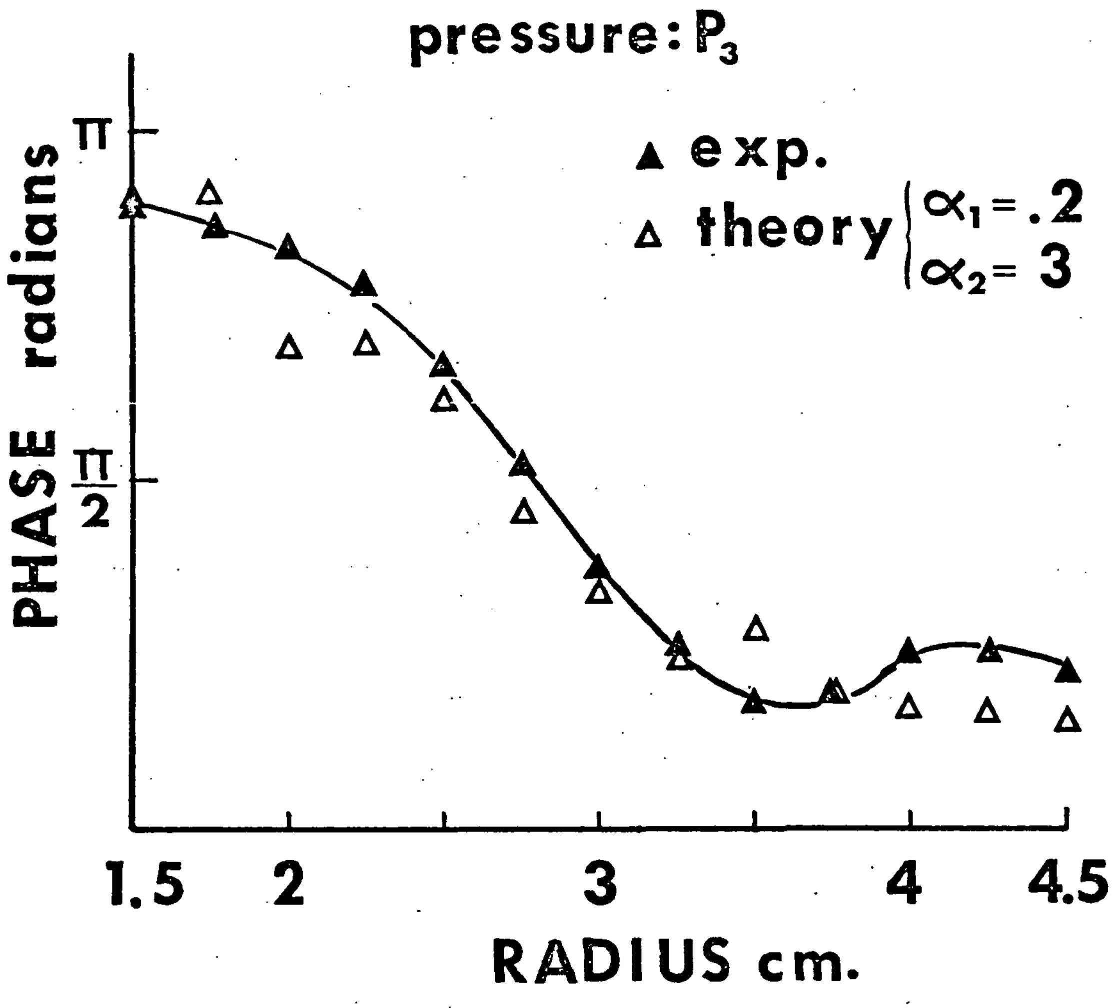

Figure 34

Phase vs. radius. Calculated from (III-11) α_1; $r \leq 2$ cm, α_2; $r > 2$ cm. Neutral pressure parameter

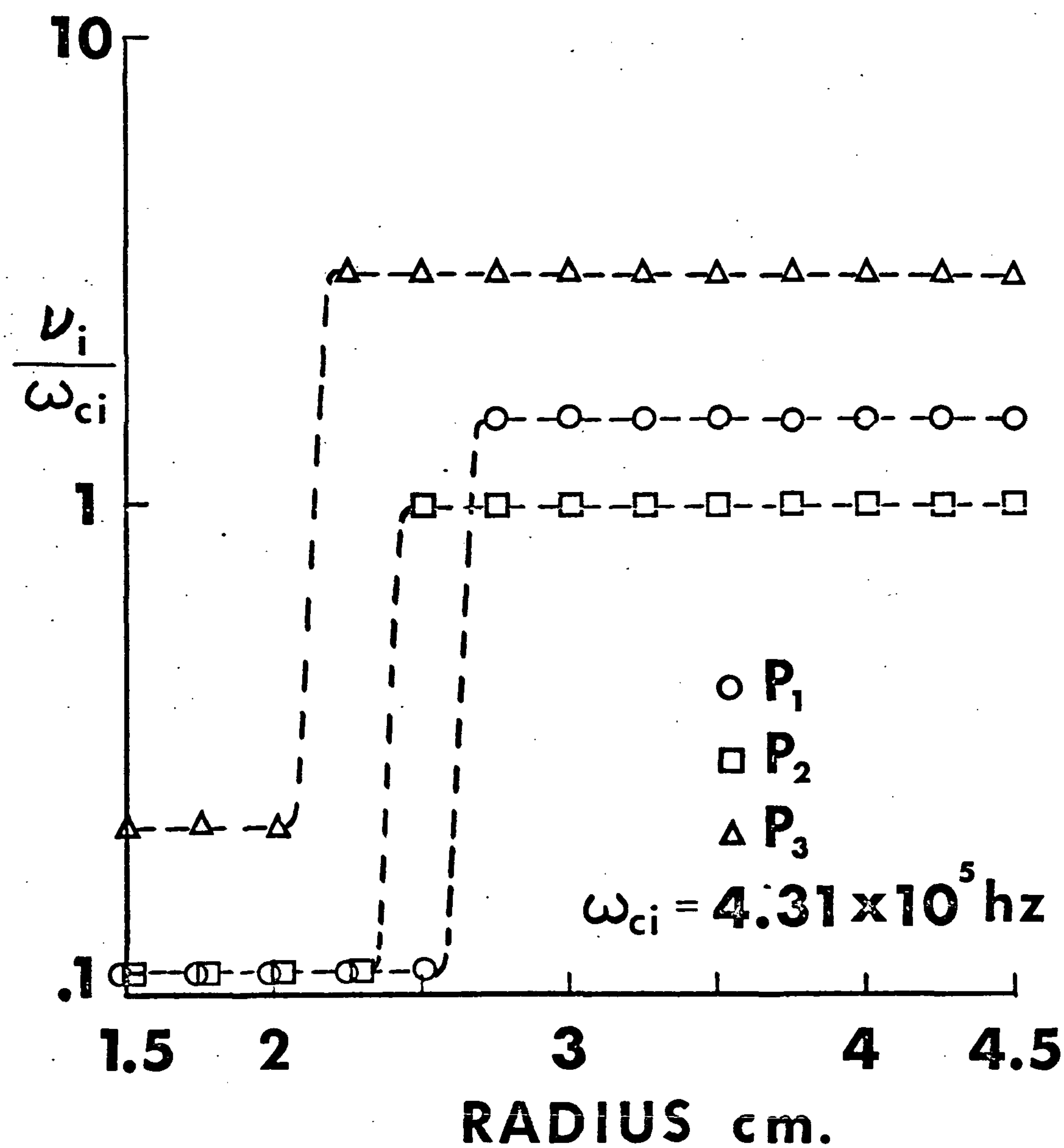

Figure 35

Collision frequency vs. radius. Neutral pressure parameter.

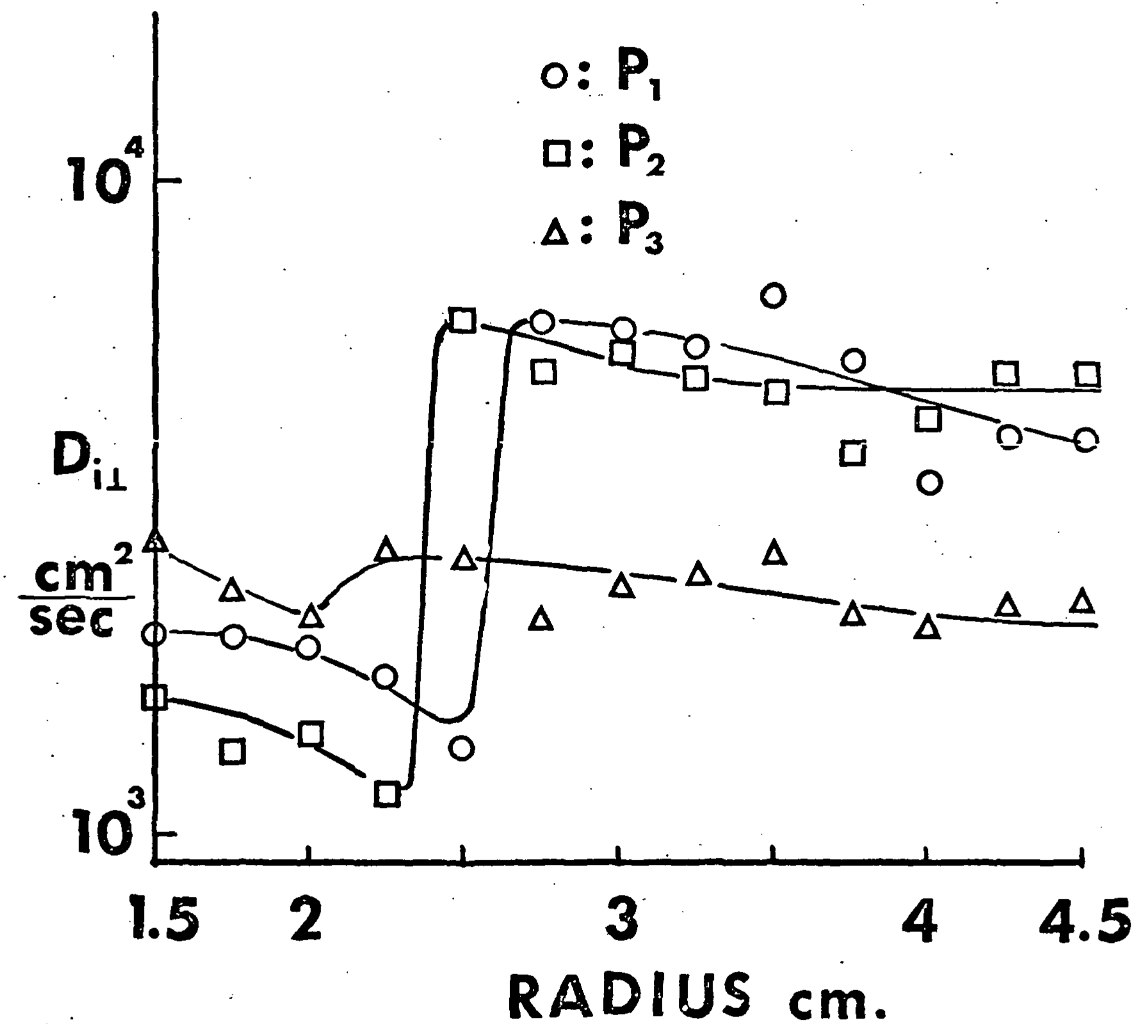

Figure 36

Diffusion coefficient vs. radius. Calculated as in Fig. 27. Neutral pressure parameter

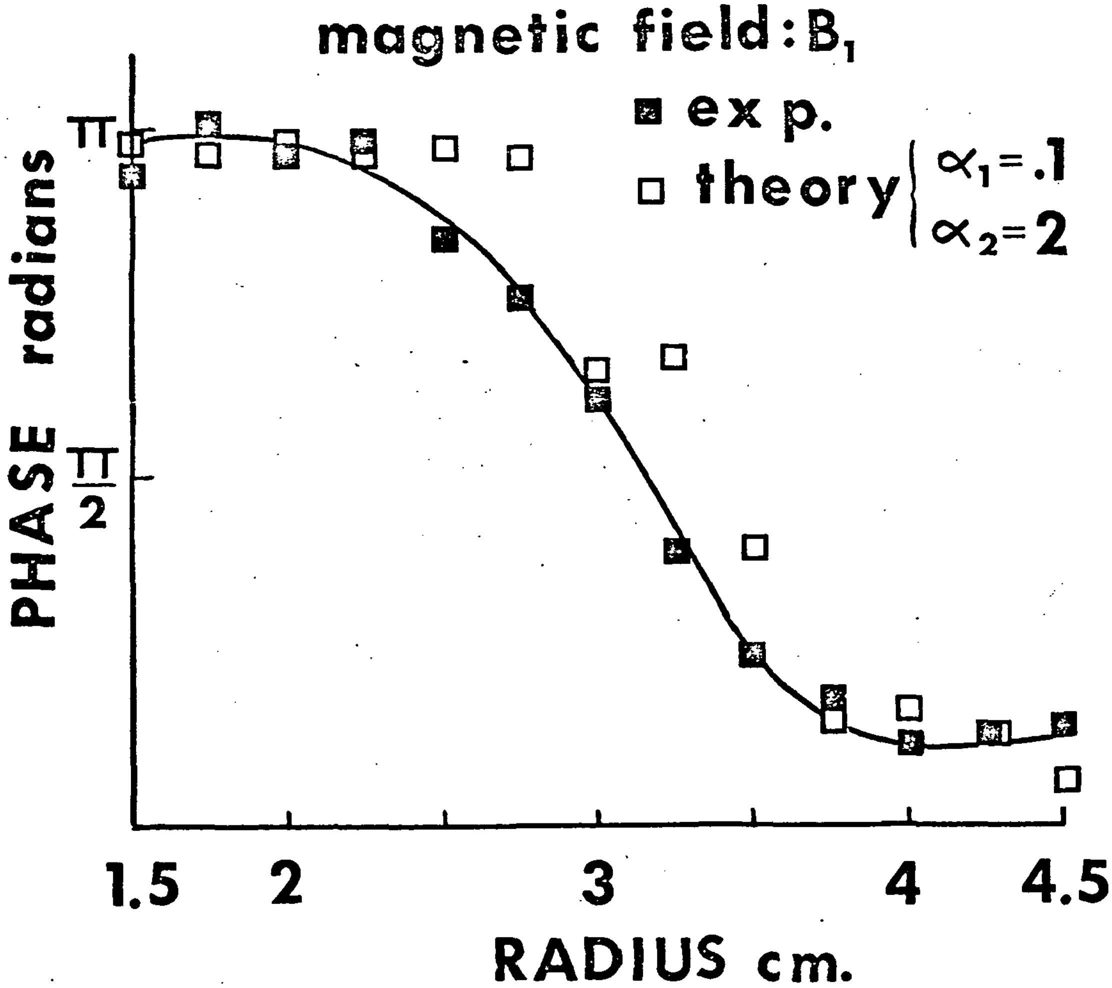

Figure 37

Phase vs. radius. Calculated from (III-11) α_1; r < 3 cm, α_2; r $\geq$ 3 cm. Magnetic field parameter variation in ν_i, as shown in Figure 39. Note that the same ratio of ν_i/ω_{ci} gives approximately the same phase difference. This means that the collision frequency increases with the magnetic field. Figure 38 contains the calculated shift for $B_3 = 2.22$ KG. This was the poorest fit obtained with few points agreeing with the experimental phase difference. The consistent points gave collision frequencies increasing with ω_{ci} as previously mentioned.

The calculated diffusion coefficients show enhancement at the same radii for different magnetic fields. An increasing magnetic field tends to confine particles closer to the core of the plasma. The enhancement decreased as B increased (Figure 40).

E) Discussion

The simple theory presented here gives some satisfactory answers to the calculation of the phase difference between the density and potential oscillations. The magnitude of ν_i/ω_{ci} is in the regime $.1 \leq \nu_i/\omega_{ci} \leq 10$. At the lower end of this range $\nu_i \approx (.1)\ \omega_{ci}$. The theory loses applicability since $\omega\tau_i \approx 1$ is now true. Increased collision frequencies where $\nu_i/\omega_{ci} \geq 1$ indicated increased diffusion. Where the phase angle is less than 90°, the diffusion is increased.

The important results are that when the phase difference is $< 90^\circ$ the diffusion is enhanced; second, when the ion-neutral collision frequency becomes important in the outer regime of the plasma, the phase difference between the density and potential oscillations decreases; and third, there is a definite shift in the position at which the plasma becomes dominated by neutral collisions as parameters varied.

The resultant variations in ν_i were much larger than expected from the experimental results. ν_i varied over 1.5 orders of magnitude in some cases. The enhanced diffusion was more consistent with our experimental

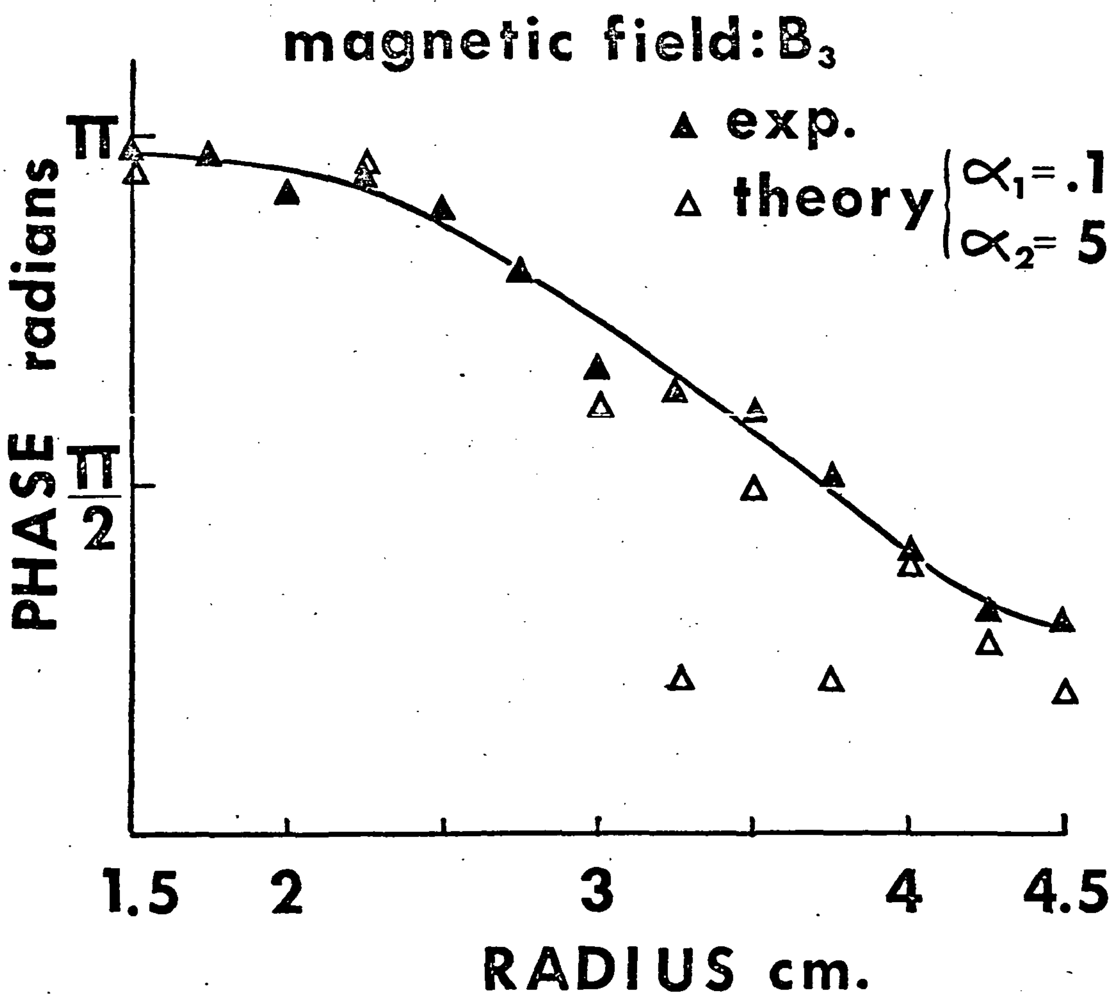

Figure 38

Phase vs. radius. Calculated from (III-11) α_1; $r < 3$ cm, α_2; $r \geq 3$ cm. Magnetic field parameter

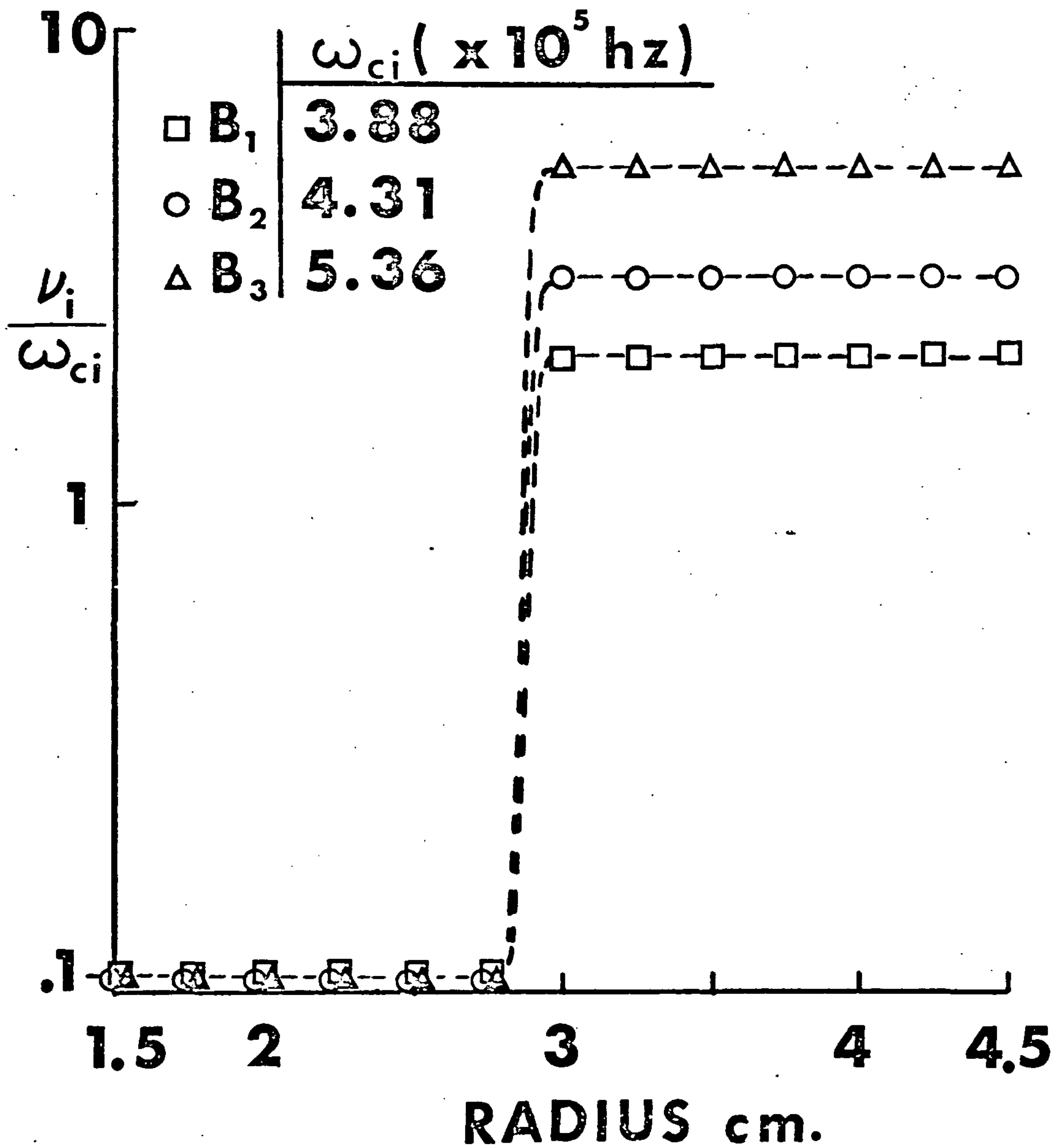

Figure 39

Collision frequency vs. radius. Magnetic field parameter

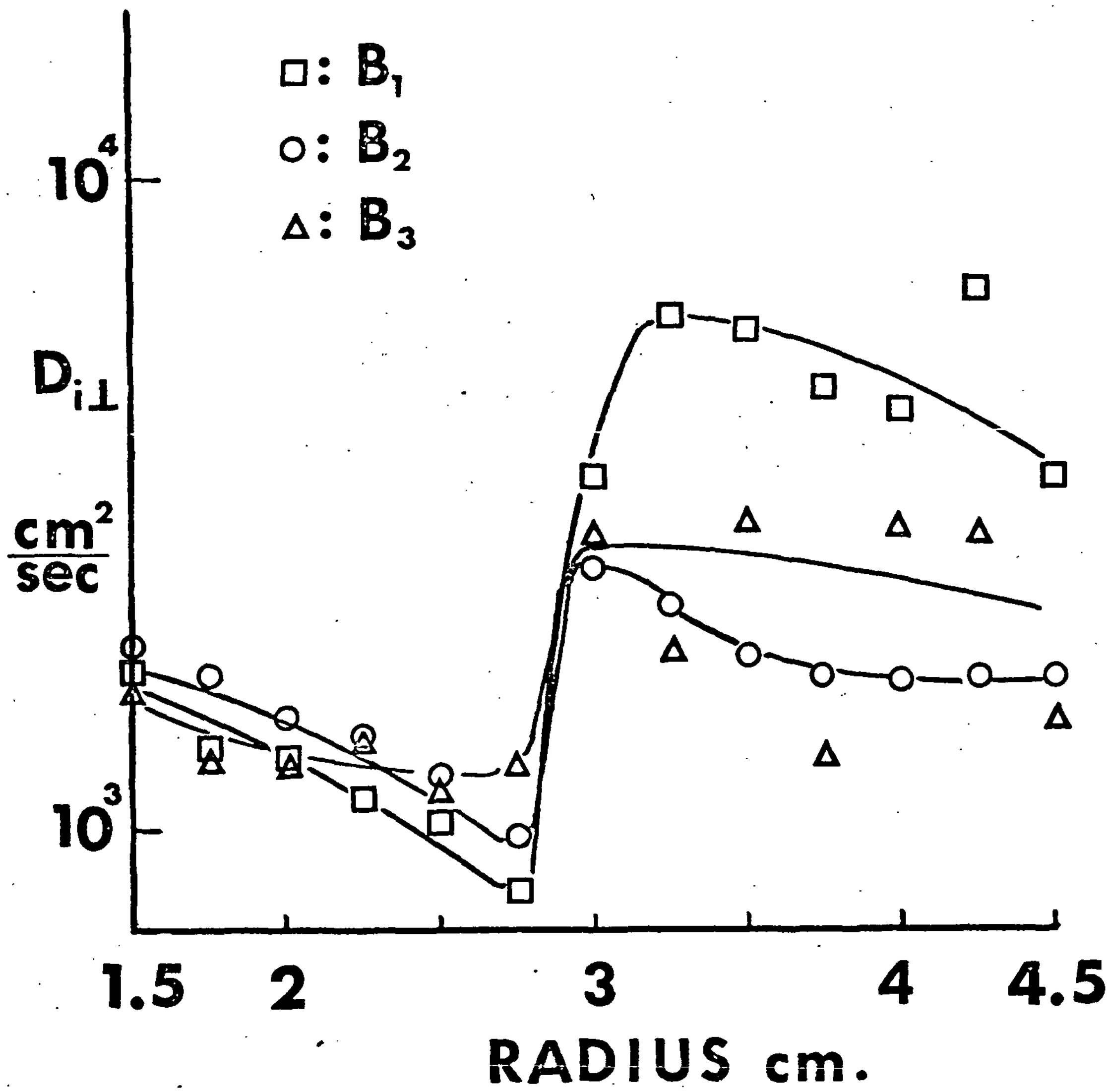

Figure 40

Diffusion coefficient vs. radius. Calculated as in Fig. 27.
Magnetic field parameter

results, the variations in $D_{i\perp}$ being factors of 4 and 5 at most.

We chose to apply the theory with two choices for α because of the limited applicability of linear theory. (1) The wave is a finite amplitude wave, and the theory is a small amplitude linear expansion. (2) Probe theory is used to determine steady state plasma parameters such as ion density. This is not such a drawback as was thought in light of Brown's conclusion (20) that probe theory gives adequate results in a magnetic field. (3) The geometry used was a slab geometry whereas the plasma is cylindrical. In spite of these problems we find that some agreement is shown between theory and experiment and that extension of this work by detailed study of linear theory in the correct geometry as well as possible nonlinear extension would improve agreement without the need for large variations in ν_i.

References

1. Chen, R. L. W., "Bounds on Fluctuations in a Homogeneous Plasma", Phy. Fluids 9, 761 (1966).

2. Fowler, T. K., "Plasma Fluctuations and the Control of Pumpout", Phy. Fluids 9, 1437 (1966).

3. Tchen, C. M., "Turbulent Diffusion of a Plasma Across a Magnetic Field", NBS Report 8435 (1966).

4. Tchen, C. M., "Spectrum of Stationary Homogeneous Magnetohydrodynamic Turbulence", Phy. Fluids 8, 1659 (1965).

5. Tchen, C. M., "Cascade Mechanism of Nonlinear Interactions Between Modes in a Turbulent Plasma", IEEE Trans. on Electron Devices ED-17, 247 (1970).

6. Golubev, V. S., "Investigation of Charge Diffusion in Ionized Gases by The Diffusion Wave Technique", Sov. Phy. JETP 6, 1399 (1963).

7. Flannery, D. L. and Brown, S. C., "Alternating Current Diagnostic Study of Diffusion in a Highly Ionized Plasma in a Magnetic Field", Phy. Flu. 13, 1066 (1970).

8. Noon, J. H. and Jennings, W. C., "Instabilities and Turbulence in Highly Ionized Plasmas in a Magnetic Field", NASA Technical Report 71-1 (April 1971).

9. Roth, J. R., "Experimental Study of Spectral Index, Mode Coupling and Energy Cascade in a Turbulent, Hot-Ion Plasma", NASA Technical Memorandum NASA TMX-52919, Presented at 12th Annual Meeting of the Plasma Physics Division of the American Physical Society, Washington, D. C., Nov. 1970.

10. Tsytovich, V. N., "Stochastic Processes in Plasma", presented at the 9th International Conference on Phenomena in Ionized Gases, Buchavest, Romania (1969).

11. Gunshor, R. L., Noon, J. H., and Holt, E. H., "Correlation Measurements Ion Acoustic Waves In Highly Ionized Plasmas", Phys. Fluids 11, 1763, 1968.

12. Noon, J. H., and Jennings, W. C., "Instabilities and Turbulence In Highly Ionized Plasmas In A Magnetic Field", Semi Annual Status Report, NASA Grant No. 33-018-137, April 1971.

13. Hendel, H. W., Chu, T. K., and Politzer, P. A., "Collisional Drift Waves - Identification, Stabilization and Enhanced Plasma Transport" Phys. Fluids 11, 2426, 1968.

14. Chung, K., and Rose, D. J., "Low Frequency Fluctuations in a Weakly Turbulent Hollow Cathode Discharge Plasma", Proceedings, Symposium on Turbulence of Fluids and Plasmas, Polytechnic Institute of Brooklyn, April 16-18, 1968.

15. Chen, F. F., "Excitation of Drift Instabilities in Thermionic Plasmas", Plasma Physics (J. of Nuclear Energy Part C) 7, 399, 1965.

16. Motley, R. W. and Ellis, R. F., "Measurement of Drift Wave Potential Oscillations in the Presence of Temperature Oscillations", MATT-793, Princeton Plasma Physics Laboratory, July 1970.

17. Aldridge, R. V., and Keen, B. E., "Rotationally Convected Drift Wave Instability in an Inhomogenous Plasma Column", Plasma Physics, 12, 1, 1970.

18. Walsh, J., "Drift Wave Fluctuations and Anomalous Diffusion in a Fully Ionized Cesium Plasma", Columbia University, E. Sc. D. Thesis, 1969.

19. Chen, F. F., "Effect of Temperature Gradients in Thermionic Plasmas", Phys. Fluids, 9, 2534 1966.

20. Brown, I. G. Compher, A. B., and Kunkel, W. B. "Response of a Langmuir Probe in a Strong Magnetic Field", Phys. Fluids 14, 1377, 1971.